

Slider-Block Friction Model for Landslides: Implication for Prediction of Mountain Collapse

A. Helmstetter¹, D. Sornette^{2–4}, J.-R. Grasso¹, J. V. Andersen^{2,5}, S. Gluzman⁴ and V. Pisarenko⁶

¹ LGIT, Observatoire de Grenoble, Université Joseph Fourier, France

² LPMC, CNRS UMR 6622 and Université de Nice-Sophia Antipolis
Parc Valrose, 06108 Nice, France

³ Department of Earth and Space Sciences

University of California, Los Angeles, California 90095-1567

⁴ Institute of Geophysics and Planetary Physics

University of California, Los Angeles, California 90095-1567

⁵ U. F. R. de Sciences Economiques, Gestion, Mathématiques et Informatique,
CNRS UMR7536 and Université Paris X-Nanterre

92001 Nanterre Cedex, France

⁶ International Institute of Earthquake Prediction Theory and Mathematical Geophysics

Russian Ac. Sci. Warshavskoye sh., 79, kor. 2, Moscow 113556, Russia

Abstract

Accelerating displacements preceding some catastrophic landslides has been found empirically to follow a time-to-failure power law, corresponding to a finite-time singularity of the velocity $v \sim 1/(t_c - t)$ [Voight, 1988]. Here, we provide a physical basis for this phenomenological law based on a slider-block model using a state and velocity dependent friction law established in the laboratory and used to model earthquake friction. This physical model accounts for and generalizes Voight's observation: depending on the ratio B/A of two parameters of the rate and state friction law and on the initial frictional state of the sliding surfaces characterized by a reduced parameter x_i , four possible regimes are found. Two regimes can account for an acceleration of the displacement. For $B/A > 1$ (velocity weakening) and $x_i < 1$, the slider block exhibits an unstable acceleration leading to a finite-time singularity of the displacement and of the velocity $v \sim 1/(t_c - t)$, thus rationalizing Voight's empirical law. An acceleration of the displacement can also be reproduced in the velocity strengthening regime, for $B/A < 1$ and $x_i > 1$. In this case, the acceleration of the displacement evolves toward a stable sliding with a constant sliding velocity. The two others cases ($B/A < 1$ and $x_i < 1$, and $B/A > 1$ and $x_i > 1$) give a deceleration of the displacement. We use the slider-block friction model to analyze quantitatively the displacement and velocity data preceding two landslides, Vajont and La Clapière. The Vajont landslide was the catastrophic culmination of an accelerated slope velocity. La Clapière landslide was characterized by a strong slope acceleration over a two years period, succeeded by a restabilizing phase. Our inversion of the slider-block model on these data sets shows good fits and suggest to classify the Vajont (respectively La Clapière) landslide as belonging to the velocity weakening unstable (respectively strengthening stable) sliding regime. We cannot however exclude that La Clapière might also belong to the unstable velocity weakening regime; its deceleration observed after 1988 may then be interpreted as a change of surface properties that modifies the friction law parameters. For the Vajont landslide, this model provides good predictions of the critical time of failure up to 20 days before the collapse. Tests are also presented on the prediction of the time of the change of regime for la Clapière landslide.

1. Introduction

Landslides constitute a major geologic hazard of strong concern in most parts of the world. The force of rocks, soil, or other debris moving down a slope can devastate anything in its path. In the United States for instance, landslides occur in all 50 states and cause \$1-2 billion in damages and more than 25 fatalities on average each year. The situation is very similar with similar costs and casualty rates in the European Union. Landslides occur in a wide variety of geomechanical contexts, geological and structural settings, and as a response to various loading and triggering processes. They are often associated with other major natural disasters such as earthquakes, floods and volcanic eruptions.

Landslides sometimes strike without discernible warning. There are however well-documented cases of precursory signals, showing accelerating slip over time scales of weeks to decades (see [*Voight (ed)*, 1978] for a review). While only a few such cases have been monitored in the past, modern monitoring techniques are bound to provide a wealth of new quantitative observations based on GPS and SAR (synthetic aperture radar) technology to map the surface velocity field [*Mantovani et al.*, 1996; *Frunzeau et al.*, 1996; *Malet et al.*, 2002; *Parise, 2001*] and seismic monitoring of slide quake activity [*Gomberg et al.*, 1995; *Xu et al.*, 1996; *Rousseau, 1999*; *Caplan-Auerbach et al.*, 2001]. Derived from the civil-engineering methods developed for the safety of human-built structures, including dams and bridges, the standard approach to slope instability is to identify the conditions under which a slope becomes unstable [e.g. *Hoek and Bray, 1997*]. In this class of approach, geomechanical data and properties are inserted in finite elements or discrete elements numerical codes to predict the possible departure from static equilibrium or the distance to a failure threshold. The results of such analyses are expressed using a safety factor F , defined as the ratio between the maximum retaining force to the driving forces. According to this approach, a slope becomes unstable when $F < 1$. This approach is at the basis of landslide hazard maps.

By their nature, standard stability analysis cannot account for acceleration in slope movement [e.g. *Hoek and Brown, 1980*]. The problem is that this modeling strategy gives a nothing-or-all signal. In this view, any specific landslide is essentially unpredictable, and the focus is on the recognition of landslide prone areas. This approach is very similar to

the practice in seismology called “time-independent hazard” where earthquake prone areas are located in association with active faults for instance, while the prediction of individual earthquake is recognized to be much more difficult if not unattainable. This “time-independent hazard” essentially amounts to assume that landslides are a random (Poisson) process in time, and uses geomechanical modeling to constrain the future long-term landslide hazard. The approaches in terms of a safety factor do not address the preparatory stage leading to the catastrophic collapse, if any. In contrast, “time-dependent hazard” would accept a degree of predictability in the process, in that the landslide hazard varies with time, maybe in association with varying external forcing (rain, snow, earthquake, volcano). The next level in the hierarchy would be “landslide forecasting”, which require significant better understanding to allow for the prediction of some of the features of an impending landslide, usually on the basis of the observation of precursory signals. Practical difficulties include identifying and measuring reliable, unambiguous precursors, and the acceptance of an inherent proportion of missed events or false alarms. Other studies of landslides analyze the propagation of a landslide and try to predict the maximum runout length of a landslide [*Heim, 1932*, *Campbell, 1989; 1990*]. These studies do not describe the initiation of a catastrophic collapse.

To account for a progressive slope failure, i.e., a time dependence in stability analysis, previous works have taken a quasi-static approach in which some parameters are taken to slowly vary to account for slow changes of external conditions and/or external loading. For instance, the accelerated motions have been linked to pore pressure changes [e.g. *Vangenuchten and Derijke, 1989*; *Van Asch et al., 1999*]. According to this approach, an instability occurs when the gravitational pull on a slope overpass the resistance of a particular subsurface level. This resistance on a subsurface level is controlled by the friction coefficient of the interacting surfaces. Since pore pressure acts at the level of submicroscopic to macroscopic discontinuities, which themselves control the global friction coefficient, circulating water can hasten chemical alteration of the interface roughness, and pore pressure itself can forces adjacent surface apart. Both effect can lead to a reduction in the friction coefficient that leads, when constant loading applies, to accelerating movement. However, this explanation has not yielded quantitative method for forecasting slope movement.

Other studies proposed that (i) rates of slope move-

ments are controlled by microscopic slow cracking, and (ii) when a major failure plane is developed, the abrupt decrease in shear resistance may provide a sufficiently large force imbalance to trigger a catastrophic slope rupture [Kilburn and Petley, 2002]. Such a mechanism, with a proper law of input of new cracks, may reproduce the acceleration preceding the collapse that occurred at Vajont, Mt Toc, Italy [Kilburn and Petley, 2002].

An alternative modeling strategy consists in viewing the accelerating displacement of the slope prior to the collapse as the final stage of the tertiary creep preceding failure [Saito and Uezawa, 1961; Saito, 1965, 1969; Kennedy and Niermeyer, 1971; Kilburn and Petley, 2002]. Further progress in exploring the relevance of this mechanism requires a reasonable knowledge of the geology of the sliding surfaces, their stress-strain history, the mode of failure, the time-dependent shear strength and the piezometric water level values along the surface of failure [Bhandari, 1988]. Unfortunately, this information is not available. This mechanism is therefore used mainly as a justification for the establishment of empirical criteria of impending landslide instability. Controlled experiments on landslides driven by a monotonic load increase have been quantified by a scaling law relating the surface acceleration $d\dot{\delta}/dt$ to the surface velocity $\dot{\delta}$ according to

$$d\dot{\delta}/dt = A\dot{\delta}^\alpha, \quad (1)$$

where A and α are empirical constants [Fukuzono, 1985]. For $\alpha > 1$, this relationship predicts a divergence of the sliding velocity in finite time at some critical time t_c . The divergence is of course not to be taken literally: it signals a bifurcation from accelerated creep to complete slope instability for which inertia is no more negligible. Several cases have been quantified ex-post with this law, usually for $\alpha = 2$, by plotting the time $t_c - t$ to failure as a function of the inverse of the creep velocity (see for a review [Bhandari, 1988]). Indeed, integrating (1) gives

$$t_c - t \sim \left(\frac{1}{\dot{\delta}}\right)^{\frac{1}{\alpha-1}}. \quad (2)$$

These fits suggest that it might be possible to forecast impending landslides by recording accelerated precursory slope displacements. Indeed, for the Mont Toc, Vajont landslide revisited here, Voight [1988] mentioned that a prediction of the failure date could have been made more than 10 days before the actual failure, by using a linear relation linking the inverse velocity and the time to failure, as found from (2) for

$\alpha = 2$. Our goal will be to avoid such an a priori postulate by calibrating a more general physically-based model for the purpose of forecasting. Voight [1988, 1989] proposed that the relation (1), which generalizes damage mechanics laws [Rabotnov, 1969; Gluzman and Sornette, 2001], can be used with other variables (including strain and/or seismic energy release) for a large variety of materials and loading conditions. Expression (1) seems to apply as well to diverse types of landslides occurring in rock and soil, including first-time and reactivated slides [Voight, 1988]. It may be seen as a special case of a general expression for failure [Voight, 1988, 1989]. Recently, such time-to-failure laws have been interpreted as resulting from cooperative critical phenomena and have been applied to the prediction of failure of heterogeneous composite materials [Anifranli et al., 1995] and to precursory increase of seismic activity prior to main shocks [Sornette and Sammis, 1995; Jaume and Sykes, 1999; Sammis and Sornette, 2002]. See also [Sornette, 2002] for extensions to other fields.

Here, we focus on two case studies, La Clapière sliding system in the French Alps and the Vajont landslide in the Italian Alps. The latter landslide led to a catastrophic collapse after 70 days of recorded velocity increase. In the former case study, decades of accelerating motion aborted and gave way to a slow down of the system. First, we should stress that, as for earthquakes for instance, it is extremely difficult to obtain all relevant geophysical parameters that may be germane to a given landslide instability. Furthermore, it is also a delicate exercise to scale up the results and insights obtained from experiments performed in the laboratory to the scale of mountain slopes. Having said that, probably the simplest model of landslides considers the moving part of the landslide as a block sliding over a surface endowed with some given topography. Within such a conceptual model, the complexity of the landsliding behavior emerges from (i) the dynamics of the block behavior (ii) the dynamics of interactions between the block and the substratum, (iii) the history of the external loading (e.g. rain, earthquake). In the following, we test how the friction law of a rigid block driven by constant gravity force can be useful for understanding the apparent transition between slow stable sliding and fast unstable sliding leading to slope collapse. We develop a simple model of sliding instability based on rate and state dependent solid friction laws and use it to assess the degree to which such events can be forecasted.

Previous modeling efforts of landslides in terms of a rigid slider-block have taken either a constant friction coefficient or a slip- or velocity-dependent friction coefficient between the rigid block and the surface. A constant solid friction coefficient (Mohr-Coulomb law) is often taken to simulate bed-over bed-rock sliding. *Heim* [1932] proposed this model as an attempt to predict the propagation length of rock avalanches. In this pioneering study to forecast extreme runout length, the constant friction coefficient was interpreted as an effective average friction coefficient. In contrast, a slip-dependent friction coefficient model is taken to simulate the yield-plastic behavior of a brittle material beyond the maximum of its strain-stress characteristics. For rock avalanches, *Eisbacher* [1979] suggested that the evolution from a static to a dynamic friction coefficient is induced by the emergence of a basal gouge. Studies using a velocity-dependent friction coefficient have mostly focused on the establishment of empirical relationships between shear stress τ and block velocity v , such as $v \sim \exp(a\tau)$ [Davis *et al.*, 1990] or $v \sim \tau^{1/2}$ [Korner, 1976], however with not definite understanding of the possible mechanism [see for instance *Durville*, 1992].

Compared to previous models, the innovation considered here is to account for the interaction between the block and the underlying slope by a solid friction law encompassing both state and velocity dependence, as established by numerous laboratory experiments (see for instance [Scholz, 1990, 1998; Marone, 1998; Gomberg *et al.*, 2000] for reviews). The sliding velocities used in laboratory to establish the rate and state friction laws are of the same order, $10^{-4} - 10^2$ $\mu\text{m/s}$, than those observed for landslides before the catastrophic collapse. On the one hand, state- and velocity-dependent friction laws have been developed and used extensively to model the preparatory as well as the elasto-dynamical phases of earthquakes. On the other hand, analogies between landslide faults and tectonic faults have been noted [Gomberg *et al.*, 1995] and the use of the static friction coefficient is ubiquitous in the analysis of slope stability. However, to our knowledge, no one has yet pushed any further the analogy between sliding rupture and earthquakes and no one has used the physics of state- and velocity-dependent friction to bear on the problem of landslides and their precursory phases. Such standard friction laws have been shown to lead to an asymptotic time-to-failure power law with $\alpha = 2$ in the late stage of frictional sliding motion between two solid surfaces preceding the elasto-dynamic rupture

instability [Dieterich, 1992]. This model therefore accounts for the finite-time singularity of the sliding velocity (2) observed for landslides and rationalizes the empirical time-to-failure laws proposed by *Voight* [1988, 1990]. In addition, this model also describes the stable sliding regime, the situation where the time-to-failure behavior is absent.

In the first section, we derive the four different sliding regimes of this model which depend on the ratio B/A of two parameters of the rate and state friction law and on the initial conditions of the reduced state variable. Sections 3 and 4 analyze the Vajont and La Clapière landslides, respectively. In particular, we calibrate the slider-block model to the two landslide slip data and invert the key parameters. Of particular interest is the possibility of distinguishing between an unstable and a stable sliding regime. We also test the predictability of the failure time using different methods, and how long in advance a prediction could have been issued. The results suggest the Vajont landslide (respectively La Clapière landslide) as belonging to the velocity weakening unstable (respectively strengthening stable) sliding regime. We also investigate the alternative possibility that La Clapière might also belong to the unstable velocity weakening regime; its deceleration observed after 1988 may then be interpreted as a change of surface properties that reset the state variable from $x < 1$ to $x > 1$. Section 5 concludes.

2. Slider-Block model with state and velocity dependent friction

2.1. Basic formulation

Following [Heim, 1932; Korner, 1976; Eisbacher, 1979; Davis *et al.*, 1990; Durville, 1992], we model the future landslide as a block resting on an inclined slope forming an angle ϕ with respect to the horizontal. In general, the solid friction coefficient μ between two surfaces is a function of the cumulative slip δ and the slip velocity $\dot{\delta}$. There are several forms of rate/state-variable constitutive law that have been used to model laboratory observations of solid friction. The version currently in best agreement with experimental data, known as the Dieterich-Ruina or ‘slowness’ law [Dieterich, 1978; Ruina, 1983], is expressed as

$$\mu = \mu_0 + A \ln \frac{\dot{\delta}}{\dot{\delta}_0} + B \ln \frac{\theta}{\theta_0}, \quad (3)$$

where the state variable θ is usually interpreted as proportional to the surface of contact between asper-

ties of the two surfaces. μ_0 is the friction coefficient for a sliding velocity $\dot{\delta}_0$ and a state variable θ_0 . The state variable θ evolves with time according to

$$\frac{d\theta}{dt} = 1 - \frac{\theta\dot{\delta}}{D_c}, \quad (4)$$

where D_c is a characteristic slip distance, usually interpreted as the typical size of asperities. Expression (4) can be rewritten as

$$\frac{d\theta}{d\dot{\delta}} = \frac{1}{\dot{\delta}} - \frac{\theta}{D_c}. \quad (5)$$

As reviewed in [Scholz, 1998], the friction at steady state is:

$$\mu_S = \hat{\mu}_0 + (A - B) \ln \frac{\dot{\delta}}{\dot{\delta}_0}, \quad (6)$$

where $\hat{\mu}_0 = \mu_0 + B \ln \frac{D_c}{\theta_0 \dot{\delta}_0}$. Thus, the derivative of the steady-state friction coefficient with respect to the logarithm of the reduced slip velocity is $A - B$. If $A > B$, this derivative is positive: friction increases with slip velocity and the system is stable as more resistance occurs which tends to react against the increasing velocity. In contrast, for $A < B$, friction exhibits the phenomenon of velocity-weakening and is unstable.

The primary parameter that determines stability, $A - B$, is a material property. For instance, for granite, $A - B$ is negative at low temperatures and becomes positive for temperatures above about 300° C. In general, for low-porosity crystalline rocks, the transition from negative to positive $A - B$ corresponds to a change from elastic-brittle deformation to crystal plasticity in the micro-mechanics of friction [Scholz, 1998]. For the application to landslides, we should in addition consider that sliding surfaces are not only contacts of bare rock surfaces: they are usually lined with wear detritus, called cataclastic or fault gouge. The shearing of such granular material involves an additional hardening mechanism (involving dilatancy), which tends to make $A - B$ more positive. For such materials, $A - B$ is positive when the material is poorly consolidated, but decreases at elevated pressure and temperature as the material becomes lithified. See also section 2.4 of Scholz's book [Scholz, 1990].

The friction law (3) with (4) accounts for the fundamental properties of a broad range of surfaces in contact, namely that they strengthen logarithmically when aging at rest, and weaken (rejuvenate) when sliding [Scholz, 1998].

To make explicit the proposed model, let us represent schematically a mountain flank as a system made of a block and of its basal surface in which it is en-cased. The block represents the part of the slope which may be potentially unstable. For a constant gravity loading, the two parameters controlling the stability of the block are the dip angle ϕ between the surface on which the block stands and the horizontal and the solid friction coefficient μ . The block exerts stresses that are normal (σ) as well as tangential (τ) to this surface of contact. The angle ϕ controls the ratio of the shear over normal stress: $\tan \phi = \tau/\sigma$. In a first step, we assume for simplicity that the usual solid friction law $\tau = \mu\sigma$ holds for all times, expressing that the shear stress τ exerted on the block is proportional to the normal stress with a coefficient of proportionality defining the friction coefficient μ . This assumption expresses a constant geometry of the block and of the surface of sliding. For the two landslides that we study in this paper, a rigid block sliding on a slope with a constant dip angle is a good first order approximate of these landslide behaviors.

2.2. Solution of the dynamical equation

2.2.1. Asymptotic power law regime for $A - B < 0$. As the sliding accelerates, the sliding velocity becomes sufficiently large such that $\dot{\delta} \gg D_c/\theta$ and we can neglect the first term $1/\dot{\delta}$ in the right-hand-side of (5). This yields

$$\theta = \theta_0 \exp(-\delta/D_c), \quad (7)$$

which means that θ evolves toward zero. The friction law then reads

$$\frac{\tau}{\sigma} = \mu_0 + A \ln \frac{\dot{\delta}}{\dot{\delta}_0} - \frac{B\delta}{D_c}, \quad (8)$$

where we have inserted (7) into (3). In this equation, τ and σ result from the mass of the block and are constant. The solution of (8) is

$$\delta(t) = -\frac{AD_c}{B} \ln \left[\frac{B\dot{\delta}_0 e^{\frac{\tau}{\sigma} - \mu_0}}{AD_c} (t_c - t) \right], \quad (9)$$

where t_c is determined by the initial condition $\delta(t=0) \equiv \delta_i$:

$$t_c = \frac{AD_c}{B\dot{\delta}_0} e^{-\left(\frac{B\delta_i}{AD_c} + \frac{\tau}{\sigma} - \mu_0\right)} \quad (10)$$

The logarithmic blow up of the cumulative slip in finite time is associated with the divergence of the slip

velocity

$$\dot{\delta} = \frac{AD_c}{B} \frac{1}{t_c - t}, \quad (11)$$

which recovers (2) for $\alpha = 2$.

2.2.2. The complete solution for the frictional problem. The solution (9) is valid only for $A - B < 0$ and sufficiently close to t_c for which the slip velocity $\dot{\delta}$ is large, ensuring the validity of the approximation leading to (7). However, even in the unstable case $A - B < 0$, the initiation of sliding cannot be described by using the approximation established for t close to t_c and requires a description different from (9) and (11). Furthermore, we are interested in different situations, in which the sliding may not result always into a catastrophic instability, as for instance for the mountain slope La Clapière, which started to slip but did not reach the full instability, a situation which can be interpreted as the stable regime $A - B > 0$. The complete solution for the frictional problem is derived in Appendix A.

2.3. Synthesis of the different slipping regimes

The block sliding displays different regimes as a function of the friction law parameters and of the initial conditions. These regimes are controlled by the value of the friction law parameters, i.e., $m = B/A$ (by definition (A3)), of the initial condition x_i on θ and of the material parameter S . A and B are defined in (3) and are determined by material properties. x_i is the initial value of the reduced state variable θ defined in (A5). The parameter S is defined by (A2) and is independent of the initial conditions. As derived from the complete solution in Appendix A, the different regimes are summarized below and in Table 1 and illustrated in Figure 1.

2.3.1. For $0 < m < 1$. the sliding is always stable. Depending of the initial value for $t = 0$ of the reduced state variable x_i , the sliding velocity either increases (if $x_i > 1$) or decreases (if $x_i < 1$) toward a constant value.

2.3.2. For $m > 1$. the sliding is always unstable. When $x_i < 1$, the sliding velocity increases toward a finite-time singularity. The slip velocity diverges as $1/(t_c - t)$ corresponding to a logarithmic singularity of the cumulative slip. For $x_i > 1$, the velocity decreases toward a vanishingly small value.

2.4. Analysis of landslide observations

In the sequel, we test how this model can reproduce the observed acceleration of the displacement for Vajont and La Clapière landslides. The Vajont landslide was the catastrophic culmination of an accelerated slope velocity over a two months period [Muller, 1964]. La Clapière landslide was characterized by a strong slope acceleration over a two years period, succeeded by a restabilizing phase [Susella and Zanolini, 1996]. An acceleration of the displacement can arise from the friction model in two regimes, either in the stable regime with $m < 1$ and $x_i > 1$ or in the unstable regime with $m > 1$ and $x_i < 1$. In the first case, the acceleration evolves toward a stable sliding. In the unstable case, the acceleration leads to a finite-time singularity of the displacement and of the velocity. However, these two regimes are very similar in the early time regime before the critical time (see Figure 1). It is therefore very difficult to distinguish from limited observations a landslide in the stable regime from a landslide in the unstable regime when far from the rupture.

We assume that the friction law parameters, the geometry of the landslide and the gravity forces are constant. Within this conceptual model, the complexity of the landsliding behavior solely emerges from the friction law. We are aware of neglecting in this first order analysis any possible complexity inherent either to the geometry and rheology of a larger set of blocks, or the geometry and rheology of the substratum or the history of the external loading (e.g. earthquake, rainfalls). We invert the friction law parameters from the velocity and displacement data of the Vajont and La Clapière landslides. Our goal is (i) to test if this model is useful for distinguishing an unstable accelerating sliding characterized by $B > A$ from a stable accelerating regime occurring for $B < A$ and (ii) to test the predictive skills of this model and compare with other methods of prediction.

3. The Vajont landslide

3.1. Historical and geo-mechanical overview

On October 9, 1963, a 2 km-wide landslide initiating at an elevation of 1100-1200 m, that is 500-600 m above the valley floor, on the Mt Toc slope in the Dolomite region in the Italian Alps about 100 km north of Venice, ended up 70 days later in a 20 m/s run-away of about 0.3 km³ of rocks sliding into a dam reservoir. The high velocity of the slide triggered a

water surge within the reservoir, overtopping the dam and killing 2000 people in the village downstream.

This landslide has a rather complex history. The landslide concerned a portion of the mountain above a newly built dam reservoir. The first attempt to fill up the reservoir dam was made between March and November 1960. It induced recurrent observations of creeping motions of a large mass of rock above the reservoir, and led to several small and rather slow slides [Muller, 1964]. Lowering the reservoir water level induced the rock mass velocities to drop from the order of 40 mm/day to less than 1 mm/day. A progressive step by step approach to slowly raise the water level as well as cycling of the water level were performed in order to slowly and cautiously fill the reservoir. A second peak of creeping velocity, at about 10 mm/day, that is four time less than the first 1960 peak, was induced by the 1962 filling cycle. The 1963 filling cycle started in April 1963. From May 1963, recurrent increases of the creep velocity was measured. It ended up abruptly in the 20 m/s downward rush of a volume of 0.3 km³ of rocks slipping in the reservoir.

The Landslide geometry is a rough rectangular shape, 2 km wide and 1.3 km in length. Velocity measurements are available for four benchmarks, corresponding to four different positions on the mountain slope, respectively denoted 5, 50, 63 and 67 in the Vajont nomenclature. Benchmarks 63 and 67 are located at the same elevation in the upper part of the landslide a few hundred meters from the submittal scarp. The distance between the 2 benchmarks is 1.1 km. The benchmark 5 and 50 are 700 m downward the 63-67 benchmark level.

Figure 2 shows the velocity of the four benchmarks on the block as a function of time prior to the Vajont landslide. For these four benchmarks, the deformation of the sliding zone prior to rupture is not homogeneous, as the cumulative displacement in the period from August 2nd, 1963 to October 8, 1963 ranges from 0.8 to 4 m. However, the low degree of disintegration for distal deposit [Erismann and Abele, 2000] argue for a possible homogeneous block behavior during the 1963 sliding collapse.

It was recognized later that limestones and clay beds dipping into the valley provide conditions favorable for dip-slope failures [Muller, 1964, 1968; Broili, 1967]. There is now a general agreement on the collapse history of the 1963 Vajont landslide (see e.g., [Erismann and Abele, 2000]). The failure occurred along bands of clays within the limestone mass at depths between 100-200 m below the surface [Hen-

dron and Patton, 1985]. Raising the reservoir level increased water pore pressure in the slope flank, that triggered the clays layer failure. Final sliding occurred after 70 days of down-slope accelerating movement. The rock mass velocity progressively increased from 5 mm/day to more than 20 cm/day, corresponding to a cumulative displacement of a few meters over this 70 days period [Muller, 1964].

3.2. Analysis of the cumulative displacement and velocity data with the slider-block model parameters.

Figure 3 shows the inverse of the velocity shown in Figure 2 to test the finite-time-singularity hypothesis (2,11). Note that this figure does not require the knowledge of the critical time t_c and is not a fit to the data. The curves for all benchmarks are almost linear in this representation, in agreement with a finite-time singularity of the velocity (2) with $\alpha = 2$. It was the observations presented in Figure 2 that led Voight to suggest that a prediction could have been issued more than 10 days before the collapse [Voight, 1988]. We note that the law $\dot{\delta} \propto 1/(t_c - t)$ requires the adjustment of α to the special value 2 in the phenomenological approach [Voight, 1988] underlying (2) while it is a robust and universal result in our model leading to (11) in the velocity-weakening regime $B > A$, $m > 1$ and for a normalized initial state variable larger than 1 (see equation (11) and Table 1).

In order to invert the parameters m , D , T of the friction model and the initial condition of the state variable x_i from the velocity data, we minimize the *rms* (root-mean-square) of the residual between the observed velocity $\dot{\delta}_{obs}$ and the velocity $\dot{\delta}$ from the friction model (A8) and (A7). The constant D in (A7) is obtained by taking the derivative of the *rms* with respect to D

$$D = \frac{\sum_{t_i} \dot{\delta}(t_i) \dot{\delta}_{obs}(t_i)}{\sum_{t_i} \dot{\delta}(t_i)^2} \quad (12)$$

where the velocity $\dot{\delta}$ in (12) is evaluated for $D = 1$ in (A7). We use a simplex algorithm (matlab subroutine) to invert the three other parameters. For each data set, we use different starting points (initial parameter values for the simplex algorithm) in the inversion to test for the sensitivity of the results on the starting point.

Figure 4 shows the fits to the velocity data using the slider-block model with the state and velocity friction law (A7) and (A8). The values of

$m = B/A$ are respectively $m = 1.35$ (benchmark 5), $m = 1.24$ (benchmark 63), $m = 0.99$ (benchmark 67) and $m = 1.00$ (benchmark 50). Most values are larger than or equal to 1, which is compatible with the finite-time-singularity regime summarized in Table 1. The parameters of the friction law are very poorly constrained by the inversion. In particular, even for those benchmarks were the best fit gives $m > 1$, other models with $m < 1$ provide a good fit to the velocity with only slightly larger rms.

We have also tried to invert the friction law parameters using only data up to a time t_{max} smaller than the last available point to mimic a real-time situation. Changing t_{max} between 30 and 70 days, we obtain a large variability of the parameters. Most values m are found larger than 1 for $30 < t_{max} < 55$ days, and then become smaller than one, and return to $m \geq 1$ for 3 benchmarks when using the full velocity data. Similar fluctuations are found when using a synthetic data set generated with the friction model. We have generated a synthetic data set using the same parameters as those of the best fit of benchmark 5, and added a white noise with the same standard deviation as that of the residue of the fit of benchmark 5. Although this synthetic data set was generated with $m = 1.35$, both $m > 1$ and $m < 1$ (for 2 points over 15 points) values are obtained when inverting the parameters up to t_{max} and changing t_{max} between 30 and 70 days. However, values with $m < 1$ for this synthetic data set are much less frequent than for the Vajont velocity data in relative terms.

Figure 5 gives another representation of Figure 4 showing the inverse of the velocity as a function of time. A saturation of the velocity before the critical time can be observed for all benchmarks, which may explain the values $m < 1$ sometimes obtained by the inversion.

It is instructive to contrast these results with those obtained by fitting the cumulative displacement (rather than the velocity) with the slider-block model with the state and velocity friction law (A7) and (A8). The results are shown in Figure 6. The fitted m are respectively $m = 0.99$ (benchmark 5), $m = 0.85$ (benchmark 63), $m = 0.68$ (benchmark 67) and $m = 0.17$ (benchmark 50). These values differ significantly from those obtained by the inversion of the velocity data and, to make things worse, they all correspond to the velocity-strengthening regime $m < 1$. At first sight, these results are quite surprising since we fit the same data, the only difference being that the cumulative displacement is the integral of the velocity. We

think that the reason for these discrepancies lies in the fact that, assuming that the velocity-weakening regime $m > 1$ holds, the corresponding logarithmic dependence (9) of the displacement δ is extremely degenerate in that it predicts an acceleration of the displacement which is significant only very close to the critical time t_c . Therefore, a cross-over from a low velocity to a larger velocity described by the regime $m < 1$ may be selected by the inversion, as we witness here. This is the curse of logarithmic singularities, which are so weak as providing poor constraints, notwithstanding the a priori reduction of noise obtained by constructing a cumulative quantity. It may actually be the case that the red noise deriving from the integral of the velocity is enough to spoil the weak logarithmic singularity: the resulting correlated noise seems to select a milder behavior. We are thus led to conclude that fits to the sliding velocity which involves stronger power law singularities should be more reliable and we shall use them exclusively in our prediction tests reported below.

The alternation of phases of accelerating and decelerating velocity in the 1960-1962 period implies that some friction parameters have changed, maybe due to changes in water level, resulting in a change of sliding regime. The change of water level may have modified the material properties of the underlying solid contacts at the base of the moving rock mass [e.g. *Erismann and Abele, 2000*], therefore changing the parameter A/B from the stable to the unstable regime. Another possibility is that changes in water level have modified the population of contacts at the basis of the rock mass, therefore changing the parameters of the friction law, and changing the sliding regime from the decelerating regime to the accelerating regime. One possible simple change of the parameters of the friction law correspond to a change of the initial condition on the state variable x_i , which may induce a change of the sliding regime from the decelerating regime for $m > 1$ and $x_i > 1$ to the accelerating regime for $m > 1$ and $x_i < 1$ and vice-versa.

3.3. Predictions and ex-post skills

We present a series of attempts at predicting in advance the critical time t_c of the catastrophic Vajont landslide instability. These attempts rely solely on the analysis of the four benchmarks velocity data up to various times $t_{max} < t_c$ mimicking a real-time situation. Therefore, we truncate the data at some time $t_{max} < t_c$ and use only the data up to t_{max} . Our goal is i) to investigate whether a prediction in ad-

vance could have been issued, as suggested by *Voight* [1988], ii) to establish the reliability and the precision limits of such predictions and iii) to test various prediction schemes that we have developed in the recent past for other applications or specifically for this problem. We use and compare 3 methods to predict the critical time $t_c = 69$ days of the collapse

- the slider block model with the state and velocity friction law described above;
- an approximation of the slider block model based on the functional renormalization method described below;
- a simple finite-time singularity (2) with $\alpha = 2$ as proposed by *Voight* [1988].

3.3.1. Prediction using the slider-block model with the state and velocity friction law. The prediction of the critical time t_c is obtained by fitting the slider-block model on the velocity time series of the four benchmarks up to a time t_{\max} . For $m \geq 1$, t_c is the time of the divergence. The divergence of the velocity exists only in the unstable regime $m > 1$. Therefore, we choose the best fit with $m > 1$, even if the best model gives sometimes $m < 1$.

3.3.2. Functional renormalization of the friction law. We are dealing with noisy time series with relatively few data points for which the detection of a singularity is a difficult task. Rather than using the full solution of a model assumed to be a good representation of reality as done in the previous sections, it may be profitable to develop prediction schemes that are less constrained by the necessarily restricting physical assumptions underlying the model and that are more specifically designed from a mathematically point of view to be resilient to noise and to the scarcity of data. Such a method is the so-called functional renormalization method, which constructs the extrapolation for future time $t > t_{\max}$ from a resummation of the time series represented by a simple polynomial expansion in powers of time t . Its mathematical foundation has been developed in a series of papers [*Yukalov and Gluzman*, 1997; *Gluzman and Yukalov*, 1997, 1998]. The application of this method to detect and predict finite-time singularities has been already investigated by *Gluzman et al.* [2001] and *Gluzman and Sornette* [2002]. We refer to these papers for a presentation of the method and restrict ourselves here to the concrete application of the method to the friction law (A7) and (A8).

The first input of the functional renormalization approach is an expansion of the variable to be predicted in increasing powers of time. In our case, we use the functional renormalization approach to provide an approximate analytical solution of the differential equation of the friction model (A4). This method is much more efficient numerically than the numerical resolution of the differential equation (A4). The friction model (A4) gives the time evolution of the state variable from which the sliding velocity $\dot{\delta}$ derives using (A1).

The needed expansion of $y \equiv \theta/\theta_0$ in powers of time t is obtained from a Taylor expansion whose coefficients are derived from successive differentiation of (A4). Up to fourth order t^4 , calling $y_0 = \theta(t=0)/\theta_0$, we obtain

$$y_k(t) \simeq \sum_{n=0}^k a_n t^n, \quad t \rightarrow 0, \quad k = 1, 2, 3, 4, \quad (13)$$

where the coefficients a_n are given in the Appendix B as a function of the friction parameters and of the initial condition.

The functional renormalization approach is in principle able to derive an extrapolation to the future from the form (13). However, in order to obtain an optimal stabilization, it is essential to incorporate as much available information as possible. In particular, in our case, we know the functional form of the dependence of the state variable as a function of time in the asymptotic regime (large times for $m < 1$ and close to the singularity for $m > 1$). Therefore, the second input of our implementation of the functional renormalization approach is the following. For $m < 1$, in a long-time limit, it is easy to show that equation (A4) has an asymptotic solution in the form,

$$y_{t \rightarrow \infty}(t) \simeq y^* + A_1 \exp\left(-\frac{t}{t^*}\right) + A_2 \exp\left(-\frac{2t}{t^*}\right) + \text{h.o.t.} \quad (14)$$

where $1/t^* = (1-m)/T = (1-m)(S\theta_0)^{1/(1-m)}$ was already defined in (A15) and h.o.t. stands for higher-order terms. The coefficients A_1 and A_2 are unspecified at this stage and can be determined using the crossover technique of *Gluzman and Yukalov* [1998], in order to optimize the stability of the solution. For $m \geq 1$, the asymptotic expression as $t \rightarrow t_c$ is of the form (A10), but we shall allow the prefactor and t_c to be adjusted to ensure maximum stability. Specifically, the determined value of t_c will be a primary result of the crossover technique.

Our goal is thus to construct a function $y(t)$ which

incorporates the short and long time asymptotics of the solution as given by expressions (13) and (14) for $m < 1$ and by (13) and (A10) for $m \geq 1$, while possibly departing from it at intermediate times to allow for a maximum stability. The general mathematical formulas that are solution of this problem are given in Appendix B for the two cases $m < 1$ and for $m \geq 1$ respectively.

For the application to the Vajont landslide, and for each “present time” t_{\max} , we assume that $m > 1$ so that t_c exists and we fit the expression of the fourth-order approximate $y_4^*(t)$ given by (B18) to the velocity of each of the four benchmarks, extract the corresponding parameters and put them in equation (B19) for the critical time t_{c4} . We stress that the function thus reconstructed is essentially indistinguishable with the naked eye from the fit with the slider-block friction model. Solving (B19) for t_{c4} allows us to construct the predicted critical time as a function of the “present time” t_{\max} . We also estimate the value of m as a function of t_{\max} . Apart from some large jumps that may be attributed to the sensitivity of specific noisy points as t_{\max} is scanned, we observe that most fits are compatible with a value of m in the range $1.3 - 1.5$.

3.3.3. Finite-time singularity (2) with $\alpha = 2$. We use a simple linear regression of the inverse of the velocity as a function of time, as proposed by *Voight* [1988]. We have found that, in order to have more stable parameters, it is necessary to give less weight to the early times where the velocity is small and contains little information on the critical time. We find that weighting each data point proportionally to its velocity seems close to optimal. The critical time t_c is then given as the time at which the fitted straight line of the $1/\dot{\delta}$ data intersects with the time axis. Recall that a linear relation between $1/\dot{\delta}$ and time t is equivalent to a power law singularity of the velocity $\dot{\delta} \sim 1/(t_c - t)$, as discussed previously, which is expected asymptotically close to t_c for the friction model in the case $m > 1$ and $x_i < 1$.

3.3.4. Comparison of three different methods of prediction of t_c as a function of the “present time” t_{\max} . The predictions of the critical time obtained from the three methods are shown in Figure 7. A prediction for t_c with an uncertainty of a few days is obtained for the 4 benchmarks within 20 days before the catastrophic failure. The reliability of the prediction is confirmed by the coherence and agreement between the three methods. Starting approximately at $t_{\max} = 45$ days, one can observe

that, using the friction model, all four time series provide a reasonable t_c prediction which however tends to increase and to follow the value of the “present time” t_{\max} . This is unfortunately a common feature of fits to power law singularities in which the last data points close to the “present” tends to dominate the rest of the time series and produce a predicted time of singularity close to the “present time” t_{\max} [Huang *et al.*, 2000; Sornette and Johansen, 2001]. The t_c value obtained using the fourth-order approximate is always a little smaller than the t_c estimated from the exact friction model. The renormalization method is therefore a little better at early times, but the exact friction model works better at the end. The t_c value obtained by the linear regression of $1/\dot{\delta}$ is too large for small t_{\max} , because it is only an asymptotic solution of the friction model for $t \approx t_c$. However, this method provides very good estimates of t_c close to t_c .

To test whether the relative value of these three methods result from a genuine difference in their stability with respect to noise or rather reflects an inadequacy of the slider-block friction model to fit the data, we have generated a synthetic velocity time series obtained by using the slider-block friction equations with the same parameters as found in the fit to the full data set of benchmark 5 and adding white noise with the same standard deviation as that of the real data set. We then applied the three prediction methods to this synthetic data set. In principle and by construction, we should expect *a priori* that the prediction based on the slider-block friction model should always perform best since it is the *true* model. This is not what we find, as shown in Figure 8. At times far from t_c , i.e. $40 \text{ days} < t_{\max} < 60 \text{ days}$, the friction model is the best, as expected. However, the prediction based on the asymptotic linear relation between $1/\dot{\delta}$ and time t is slightly better than the friction model, starting approximately 9 days before the landslide.

The overall conclusion is that the least sophisticated approach, that is the linear regression of $1/\dot{\delta}$, seems to perform as well as or slightly better than the sophisticated renormalization method or the exact friction model for “present times” sufficiently close to the critical time t_c . For times further away from t_c , the renormalization method and the exact friction model are better. Although the corresponding power-law is only an asymptotic solution of the friction model for times close to t_c , the linear regression of $1/\dot{\delta}$ gives significantly better predictions than the exact model or the renormalization method. However,

we must keep in mind that the use of the linear regression of $1/\dot{\delta}$ as a function of time contains two hidden and rather strong assumptions: the power law and the value of its exponent. Without the slider-block friction model, these assumptions are just guesses and are a priori unjustified.

4. La Clapière landslide: the aborted 1986-1987 peak acceleration

We now report results on another case which exhibited a transient acceleration which did not result in a catastrophic failure but re-stabilized. This example provides what is maybe an example of the $m < 1$ stable slip regime, i.e. $B < A$, as interpreted within the friction model.

4.1. Historical and geo-mechanical overview

4.1.1. Geo-mechanical setting and Displacement history: 1950-2000. La Clapière landslide is located at an elevation between 1100 m and 1800 m on a slope that culminates at 3000 m high and has a width of about 1000 m. The summit of the main scarp ranges in elevation between 1550 and 1735 m. Figure 9 shows La Clapière landslide in 1979 before the acceleration of the displacement, and in 1999 after the end of the crisis. The volume of mostly gneiss rocks implied in the landslide is estimated to be around 50×10^6 m³. At an elevation of about 1300 m, a 80 m thick bed provides a more massive and relatively stronger level compared with the rest of relatively weak and fractured gneiss. The two lithological entities are characterized by a change in mica content which is associated with a change of the peak strength and of the elastic modulus by a factor two [Follacci *et al.*, 1990, 1993]. Geomorphological criteria allow one to distinguish three distinct sub-entities within the landslide, NW, Central and SW respectively [Follacci *et al.*, 1988].

There is some historical evidence that the rock mass started to be active before the beginning of the 20th century. In 1938, photographic documents attest the existence of a scarp at 1700 m elevation [Follacci, 2000]. In the 1950-1980 period, triangulation and aerial photogrammetric surveys provide constraints on the evolution of the geometry and the kinematics of the landslide (Figure 10). The displacement rate measured by aerial photogrammetric survey increased from 0.5 m/years in the 1950-1960 period to 1.5 m/years in the 1975-1982 period [Follacci *et al.*, 1988]. Starting in 1982, the displacements of 43 benchmarks have

been monitored on a monthly basis using distance meters [Follacci *et al.*, 1988, 1993; Susella and Zanolini, 1996]. The displacement data for the 5 benchmarks in Figure 9 is shown in Figure 11. The velocity is shown in Figure 12. The rock mass velocities exhibited a dramatic increase between January 1986 and January 1988, that culminated in the 80 mm/day velocity during the 1987 summer and to 90 mm/day in October 1987. The homogeneity of benchmark trajectories and the synchronous acceleration phase for most benchmark, attest of a global deep seated behavior of this landslide [e.g. Follacci *et al.*, 1988]. However, a partitioning of deformation occurred, as reflected by the difference in absolute values of benchmark displacements (Figure 11). The upper part of the landslide moved slightly faster than the lower part and the NW block. The observed decrease in displacement rate since 1988 attest of a change in landsliding regime at the end of 1987 (Figure 11).

4.1.2. Correlations between the landslide velocity and the river flow. The velocity displays large fluctuations correlated with fluctuations of the river flow in the valley as shown in Figure 13. There is a seasonal increase of the slope velocity which reaches a maximum V_{\max} of the order of or less than 30 mm/days. The slope velocity increases in the spring due to snow melting and over a few days after heavy precipitations concentrated in the fall of each year [Follacci *et al.*, 1988; Susella and Zanolini, 1996]. During the 1986-1988 period, the snow melt and rainfalls were not anomalously high but the maximum value of the velocity, $V_{\max} = 90$ mm/day, was much larger than the velocities reached during the 1982-1985 period for comparable rainfalls and river flows [Follacci *et al.*, 1988; 1993]. This strongly suggests that the hydrological conditions are not the sole control parameters explaining both the strong 1986-1987 accelerating and the equally strong slowdown in 1988-1990. During the interval 1988-1990, the monthly recorded velocities slowed down to a level slightly higher than the pre-1986 values. Since 1988, the seasonal variations of the average velocity never recovered the level established during the 1982-1985 period [Follacci *et al.*, 1993; David and ATM, 2000]. Rat [1988] derives a relationship between the river flow and the landslide velocity by adjusting an hydrological model to the velocity data in the period 1982 to 1986. This model tuned to this time period does not reproduce the acceleration of the velocity after 1986.

In order to study quantitatively the effect of the

precipitations on the landslide velocity, we need to remove the long-term fluctuations of the velocity that may not correlated to changes in the precipitations. We divide the data of benchmark 10 of La Clapière into three different intervals: [1982.917, 1987.833], [1987.833, 1991.25] and [1991.25, 1995.5]. The initial values of the time and of the displacement are fixed to 0 at the beginning of each time period. In the first interval, the velocity rises (with fluctuations); in the second interval, the velocity decreases (with fluctuations); in the third interval, the velocity fluctuates around a constant. We used non-linear Least-Square fits with different fitting functions separately within each interval. The results of the fits are the following.

1. In the first interval [1982.917, 1987.833], we fit the displacement by $d(t) = a(|1 - t/t_0|^{-b} - 1)$ with $a = 8.96$, $b = 1.01$ and $t_0 = 6.26$ years.
2. For the second interval [1987.833, 1991.25], we use the same functional form with $a = 10.42$, $b = 0.4106$ and $t_0 = -0.1081$. The negative value of t_0 implies a decay of the displacement.
3. For the third interval [1991.25, 1995.5], we use a fit by $d(t) = at^b$ which has only two parameters $a = 7.4687$ and $b = 0.989$.

The goodness of fit is very good in all three regimes: the standard deviations of the residuals being of the order of 0.4 while the magnitude of the displacement is about 30, this yields a signal-over-noise ratio of 75, which is very good.

Figure 14 compares the the Burg's power spectrum of the flow rates of the Tinée river and of the detrended velocity residuals. The Burg spectrum is a kind of smoothed FFT (fast-Fourier transform) obtained by approximating the true spectrum by that of an autoregressive process of a finite order. The top panel of figure 14 exhibits the Burg's power spectrum of the flow rates of the Tinée river on the 1982-1988 and on the 1988-1996 periods, which are proxies of the cycle of precipitations and snow melting. The bottom panel of figure 14 shows the Burg's power spectrum of the detrended velocity residuals for these two periods.

In the first time interval 1982-1988, a strong peak at the period of 1 year appears both for the velocity residuals and for the river flow. This correspondence is confirmed by the strong cross-correlation between the river flow and the landslide velocity, which is also directly apparent visually in Figure 13. Let us use the language of system theory and consider the river flow as an input (or a forcing) and the landslide velocity as

an output of the system. These observations of a common spectral peak and of a strong cross-correlation are then compatible with a view of the system as being linear or only weakly non-linear.

In contrast, the (linear) correlation between the river flow input and the landslide velocity output disappears in the second time interval 1988-1996, as can be seen from the absence of a spectral peak at the period of 1 years and a very weak peak at the period 6 months ($f = 2 \text{ year}^{-1}$) in the (output) landslide velocity spectrum compared with the two strong peaks at the same periods of 1 years and 6 months observed in the (input) river flow spectrum. This breakdown of linear correlation seems to be associated with the birth of a strong peak close to the sub-harmonic period of 2 years ($f = 0.5 \text{ year}^{-1}$), which is absent in the river flow rate. This suggests the following interpretation. Frequency doubling or more generally frequency multiplications are the results of simple nonlinearities. Indeed, higher frequency overtones in river runoff is very common feature of hydrological regime (see for instance [Pisarenko *et al.*, 2002]). In contrast, the creation of sub-harmonics requires bifurcations or period-doubling, for instance involving nonlinear processes with time delays. It thus seems that the input of rain and snow melting is transformed by the system during the second time interval via the process of such delayed period-doubling nonlinearities. It is intriguing that the change of sliding regime to a reduction of velocity in the second time interval seems here to be associated with such a sub-harmonic non-linearity, which could be the result of a change of topology of the block structures (through fragmentation) and of the solicitation of novel fresh surfaces of sliding.

4.1.3. Fracturing patterns contemporary to the 1986-1987 accelerating regime. In 1985-1986, a transverse crack initiated in the upper part of the NW block. It reaches 50 m of vertical offset in 1989. The maximum rate of change of the fracture size and of its opening occurred in 1987 [Follacci *et al.*, 1993]. This new transverse crack uncoupled the NW block from the upper part of the mountain, which moved at a much smaller velocity below 1 mm/day since 1985-86 [Follacci *et al.*, 1993] (Figures 9 and 15). Since summer 1988, an homogenization of the surface morphological faces and a regression of the main summit scarp were reported. The regression of the summit scarp was observed as a new crack started to open in September 1988. Its length increased steadily to reach 500 m and its width reached 1.75 m in November 1988. Accordingly, the new el-

evation of main scarp in the SE block reaches 1780 m. This crack, which defined a new entity, that is the upper SE block, has remained locked since then (Figures 9 and 15).

4.1.4. Current understanding of the La Clapière acceleration. On the basis of these observations and simple numerical models, an interpretative model for the 1986-1988 regime change was proposed by *Follacci et al.*, [1993] [see also for a review *Susella and Zanolini*, 1996]. In fact, these models do not explain the origin of the acceleration but rather try to rationalize kinematically the different changes of velocity and why the acceleration did not lead to a catastrophic sliding but re-stabilized. The reasoning is based on the fact that the existing and rather strong correlation between the river flow in the valley at the bottom and the slope motion (see Figure 13) is not sufficient to explain both the de-stabilizing phase and its re-stabilization. This strongly suggests that the hydrological conditions are not the sole control parameters explaining both the strong 1986-1987 accelerating and the equally strong slowdown in 1988-1990.

Follacci et al. [1988, 1993] argue that the failure of the strong gneiss bed in the NW block was the main driving force of the acceleration in 1986-1987. According to this view, the failure of this bed induced changes in both the mechanical boundary conditions and in the local hydro-geological setting (Figure 15). Simultaneously, the development of the upper NW crack, that freed the landslide from its main driving force, appears as a key parameter to slow down the accelerating slide. The hypothesized changes in hydrological boundary conditions can further stabilize the slide after the 1986-1987 transient leak off.

Several works have attempted to fit the velocity time series of La Clapière landslide and predict its future evolution, in a spirit similar to the Vajont landslide discussed above. The displacement of different benchmarks over the 1982-1986 period has been analysed. An exponential law has been fitted to the 1985-1986 period [*Vibert et al.*, 1988]. Using the exponential fit and a failure criterion that the landslide will collapse when the velocity reaches a given threshold, the predicted collapse time for the landslide ranges from 1988 for NW benchmark to 1990 for the SE benchmarks. Plotting the inverse of the velocity as a function of time as in (2) has been tried, hoping that this law holds with $\alpha = 2$ providing a straightforward estimation of t_c . This approach applied to La Clapière velocity data predicts a collapse in 1990

for the upper NW part and in 1988-1989 for the SE part of the landslide. To remove the fluctuations of the velocity induced by changes in river flow, an ad-hoc weighting of the velocity data was used by [*Vibert et al.*, 1988]. An attempt to more quantitatively estimate the relation between the river flow and the landslide velocity was proposed by [*Rat*, 1988]. *Rat* [1988] stresses the importance of removing the fluctuations of the velocity induced by changes in the river flow before any attempt to predict the collapse time.

4.2. Analysis of the cumulative displacement and velocity data with the slider-block model

The simple rigid block model defined with a single block and with velocity and state dependent friction law cannot account for what happened after the velocity peak, without invoking additional ingredients. Departure from the model prediction can be used as a guide to infer in-situ landslide behavior. Recall that, during the interval 1988-1990, the monthly recorded velocities slowed down to velocity 6 times smaller than the 1987 peak values. This deceleration cannot be explained with the friction model using constant friction parameters. Indeed, for $B/A = m < 1$, under a constant geometry and fixed boundary conditions, the velocity increases and then saturates at its maximum value. In order to explain the deceleration of the landslide, one needs to invoke either a change of material properties embodied for example in the parameter $m = B/A$ or a change of the state variable θ that describes the duration of frictional contacts, maybe due to a change in the sliding surfaces.

We have not attempted in this study to fit both the accelerating and the decelerating phases with the slider-block model due to the large number of free parameters it will imply relatively to the small number of points available. Further modeling would allow block partitioning, fluctuations of the slope angle and change with time of the friction parameters. Our purpose is here to point out how different landsliding regimes can be highlighted by the introduction of a velocity and state friction law in this basic rigid block model. It would also be interesting to add a periodic forcing to our models to better capture the time-dependence of the velocity and study its possible nonlinear consequences. This is left for a future work, together with a complete description of the three time intervals by the slider-block friction model.

4.2.1. La Clapière sliding regime: 1982-1987. We fit the monthly measurements of the displacement of several representative benchmarks with

the slider-block friction model. In the sequel, we will show results for benchmark 10 which is located in the central part of the landslide (Figure 9), and which is representative of the average landslide behavior during the 1982-1995 period [Follacci, personal communication 2001]. We have also obtained similar results for benchmark 22.

We consider only the accelerating phase in the time interval [1982.92; 1987.9]. As for the Vajont landslide, the inversion provides the values of the parameters m , T , D , and the initial condition x_i of the state variable. The best fit to the displacement of benchmark 10 is shown in Figure 16. The model parameters are $m = B/A=0.98$ and the initial value of the reduced state variable is $x_i = 39$. While m is very close to one, the value of x_i significantly larger than 1 argues for La Clapière landslide to be in the stable regime (see Figure 1 and Table 1). Similar results are obtained for the other benchmarks. Since the landslide underwent different regimes, it is important to perform these inversions for different time periods, that is, the fits are done from the first measurement denoted time $t = 0$ (year 1982.92) to a later $t = t_{\max}$, where t_{\max} is increased from approximately 2 years to 5 years after the initial starting date. This last time $t \approx 5$ years (end of 1987) corresponds to the time at which the slope velocity reached its peak. For all inversions except the first two point with $t_{\max} \approx 2$ yrs, the best fit always select an exponent $0 < m < 1$ and an initial state variable $x_i \gg 1$, corresponding to a stable asymptotic sliding without finite-time singularity. For $t_{\max} < 4$ years (that is, using data before the end of 1986), a few secondary best solutions are found with very different values, from $m = -3000$ to $m = 29$, indicating that m is poorly constrained. We have also performed sensitivity tests using synthetic data sets generated with the friction model with the same parameters as those obtained for La Clapière. These tests show that a precise determination of m is impossible but that the inversion recovers the true regime $m < 1$.

The transition time (defined by the inflection point of the velocity) is found to increase with t_{\max} (see Figure 17). This may argue for a change of regime from an acceleration regime to a restabilization before the time $t = 1988$ of the velocity peak. The parameters S and x_i are also not well constrained. Similar results are obtained for different benchmarks as well as when fitting the velocity data instead of the displacement. A fit to the velocity of benchmark 10 is shown in Figures 18 and 19. The velocity data show large

fluctuations, in part due to yearly fluctuations of the precipitations. The inversion is therefore even more unstable than the inversion of the displacement, but almost all points give $m < 1$ and $x_i > 1$. Such fluctuations of the inverted solution may indicate that the use of constant friction parameters to describe a period where 2 regimes interact, i.e., an accelerating phase up to 1987 followed by a decrease in sliding rate since 1988, does not describe adequately the landslide behavior for the whole time period 1983-1988. Observed changes in morphology as suggested in Figure 15 provide evidence for changes both in driving forces and in the geometry of the landslide, including possible new sliding surfaces.

4.2.2. An alternative interpretation. While a fit to the displacement or to the velocity data for the whole time period 1983-1988 suggests that the landslide was in the stable regime $m < 1$, an alternative interpretation is that the early acceleration was in the unstable regime $m > 1$ but did not reach the instability due to a change of morphology, block partition and the creation of new active surfaces of sliding. This interpretation is suggested by the plot of the inverse of the velocity shown in Figure 19, which is close to linear at early times. Over the route toward the finite-time singularity, the landslide did not succeed in accommodating the velocity increase and degenerated by changing geometry and loading conditions (block partitioning). In other words, the solution shown in Figure 16 with $m < 1$ may rather describe a transient from an unstable state to a stable regime. In particular, we cannot exclude the possibility that the surfaces have been all along characterized by the regime $B > A$ and then a change of geometry and surfaces of sliding may have reset the reduced state variable x given by expression (A5). Another possibility is that the friction parameter m has changed from $m > 1$ to $m < 1$, leading to a stable deceleration of the displacement after 1988. It is not unreasonable to conjecture that the internal stresses associated with and created by the accelerating phase may have led to its fragmentation into several sub-entities, creating fresh surfaces and resetting the state variable or the m -value characterizing the surfaces of contact. This is in qualitative agreement with field observations of new faulting patterns since 1987, which signal a change in the geometry of the landslide involving the regression of the main scarp and locked sub-entities (Figure 15). These observations provide evidence for a change in both the head driven force (mass push from the top) and the activated basal surfaces. These morphological

changes suggest that the 1987-1988 period has been a transition period for the evolution of La Clapière sliding system over the last 50 years. In the block-slider model, this amounts to modifying the variables S and θ_i and thus to reset x . In this interpretation, the change of regime observed for La Clapière could then be due to a change from $x_i < 1$ (unstable acceleration) to $x_i > 1$ (stable deceleration) (see Figure 1). This change from $x_i < 1$ to $x_i > 1$ may be interpreted as either an increase of applied shear stress, a decrease of normal stress, or an increase of the surface of contacts between the sliding surfaces. Thus, within the slider-block model, one can characterize the post 1988 landslide evolution in terms of new sliding surfaces being mobilized which are more stable than the previous ones due to more numerous and/or efficient contacts.

Appendix C explores what would have been the predicted critical time t_c estimated in real time prior to the velocity peak, according to this scenario of an unstable acceleration towards a finite-time singularity. We have seen that, while the slider-block model as well as the power law formula (2) provide excellent fits to the data, they do not lead to very stable predictions of the critical time t_c on the Vajont data as well as on synthetic tests generated in the unstable regime $m > 1$. It may thus be valuable to test the approach of [Gluzman *et al.*, 2001] in terms of a version of the functional renormalization approach already discussed in relation with the Vajont landslide. It is our hope that this approach could provide in a more robust determination of t_c .

Figure 20 compares the prediction of a fit using a polynomial of order two in time to the inverse of the velocity (panel (a)) with the prediction of the renormalization approach (panel (b)). In each panel, two curves are presented corresponding to two different starting points of the data taken into account in the predictions: the leftmost points correspond to the first date taken into account in the predictions; therefore, the predictions corresponding to the crosses \times use approximately two years fewer data than the predictions shown with the open circles. This allows us to compare the effect of missing data or alternatively the effect of a non-critical behavior at the beginning of the time series. The abscissa t_{\max} is the running “present time”, that is, the last time of the data taken into account to issue a prediction. The prediction with the polynomial shown in panel (a) of Figure 20 can be seen as an improvement in methodology over the Voight formula (2) which corresponds to a linear fit

of the inverse velocity with time for $\alpha = 2$. Comparing panels (a) and (b), the renormalization method seems to present a smaller dispersion and better convergence: in particular, about half-a-year prior to the time of the maximum realized velocity indicated by the horizontal dashed line, the prediction of this date by the renormalization method using the longer time series becomes very precise. Thus, a critical time close to the time of the velocity peak would have been predicted starting approximately half-a-year year from it. It is then not unreasonable to consider the velocity peak as a proxy for the ghost critical time, since on the approach of the later the largest internal stresses may develop and may fragment the block and modify the morphology of the landslide, thus resetting the geometry and some of the parameters of the model. In this scenario, we would thus expect that the time of the peak velocity should be not far from what would have been the critical time of catastrophic failure of the landslide.

We should however point out that the functional renormalization method used in this Appendix C does not work for the Vajont landslide because of a technical instability whose fundamental origin is not understood by these authors. Technically, the numerical instability comes from the absence of alternating signs in the polynomial expansion at early times. This technical problem thus casts some shadow on the usefulness of the approach described here which is unable to tackle the regime which is undoubtedly unstable. This limitation suggests again the importance of working with several alternative and competing models, as further discussed in the following concluding section.

5. Discussion and conclusion

We have presented a quantitative analysis of the displacement history for two landslides, Vajont and La Clapière, using a different set of techniques. We have tried to go beyond the time-independent hazard analysis provided by the standard stability analysis to include time dependent predictions. While our present inversion methods provide a single estimate of the critical time t_c of the collapse for each inversion, a better formulation should be to translate these results in terms of a probability of failure, as for instance done by Vere-Jones *et al.* [2001].

A first innovative concept proposed here was to apply to landslides the state and velocity dependent friction law established in the laboratory and used

to model earthquake friction. Our inversion of this simple slider-block friction model shows that the observed movements can be well reproduced with this simple model and suggest the Vajont landslide (respectively La Clapière landslide) as belonging to the velocity weakening unstable (respectively strengthening stable) regime. Our friction model assumes that the material properties embodied in the key parameters $m = B/A$ and/or the initial value of the state variable of the friction law control the sliding regime.

Our purpose was here to point out how different landsliding regimes can be highlighted by the introduction of a velocity and state friction law in a basic rigid block model. Even if the displacement is not homogeneous for the two landslides, the rigid block model provides a good fit to the observations and a first step towards a better understanding of the different sliding regimes and the potential for their prediction.

For the Vajont landslide, this physically-based model suggests that this landslide was in the unstable regime. The friction model provides good predictions of the time-to-failure up to 20 days before the collapse. A pure phenomenological model suggested by Voight [1988] postulating a power law finite-time singularity $v \sim 1/(t_c - t)$ with unit exponent obtains similar results. Our approach can be seen as providing a physically-based derivation of this phenomenological model as well as a generalization to capture three other possible regimes.

For la Clapière landslide, the inversion of the displacement data for the accelerating phase 1983-1888 up to the maximum of the velocity gives $m < 1$, corresponding to the stable regime. The deceleration observed after 1988 implies that, not only is la Clapière landslide in the stable regime but in addition, some parameters of the friction law have changed, resulting in a change of sliding regime from a stable regime to another one characterized by a smaller velocity, as if some healing process was occurring. Possible candidates for a change in landsliding regime include the average dip slope angle, the partitioning of blocks, new sliding surfaces and changes in interface properties. However, another possible interpretation is that this landslide was initially in the unstable regime, but did not reach the instability due to a change of geometry and of sliding surfaces. The best fit obtained with $m < 1$ for the accelerating phase 1983-1988 would then describe a transient regime between the unstable regime and the stable regime, due to a progressive change in the model parameters. This second scenario

seems less parsimonious but cannot be completely excluded.

The present work has offered the important insight and novel conceptual framework and language of the slider-block model, which can be used to classify the relative merits and performance of other models. For an assessment in real time of the upcoming risks of a catastrophic failure, one should then consider both scenarios (stable versus unstable which are encoded respectively by the range of parameters $m < 1$ and $m > 1$ in the slider-block model) and test the data using the available associated theoretical models, some of which have been presented in this paper. Such an approach in terms of multiple scenarios [Smith *et al.*, 1999; Yukalov and Gluzman, 1999; Ziehmann *et al.*, 2000] can add a contribution to the assessment of societal risks. A systematic exploration of such approaches will extend the preliminary investigation and results offered here. In this spirit, the major innovation of the frictional slider-block model that should be explored further is to embody the two regimes (stable versus unstable) in the same physically-based framework, and to offer a way of distinguishing empirically between the two regimes, as shown by our analysis of the two cases provided by the Vajont and La Clapière landslides.

Acknowledgments. We thanks C. Scavia and Y. Guglielmi for key supports to capture archive data for Vajont and La Clapière landslide respectively. We are very grateful to N. Beeler, J. Dieterich, Y. Guglielmi, D. Keefer, J.P. Follacci, J.M. Vengeon for useful suggestions and discussions. AH and JRG were supported by INSU french grants, Gravitationnal Instability ACI. SG and DS acknowledge support from the James S. Mc Donnell Foundation 21st century scientist award/studying complex systems.

Appendix A: Derivation of the full solution of the frictional problem

1.1. Complete solution

We now provide the full solution of the frictional problem. First, we rewrite (3) as

$$\dot{\delta} = S D_c \left(\frac{\theta}{\theta_0} \right)^{-m}, \quad (A1)$$

where

$$S \equiv \frac{\dot{\delta}_0 e^{\frac{\bar{\sigma} - \mu_0}{A}}}{D_c} \quad (A2)$$

and

$$m \equiv \frac{B}{A}. \quad (A3)$$

Putting (A1) in (4) gives

$$\frac{d(\theta/\theta_0)}{dt} = \frac{1}{\theta_0} - S (\theta/\theta_0)^{1-m}. \quad (\text{A4})$$

The case $m = 1$ requires a special treatment since the dependence in θ disappears in the right-hand-side of (A4) and $\frac{d\theta}{dt}$ is constant.

For $m \neq 1$, it is convenient to introduce the reduced variables

$$x \equiv (S\theta_0)^{1/(1-m)} \frac{\theta}{\theta_0}, \quad (\text{A5})$$

and

$$D \equiv D_c (S\theta_0^m)^{\frac{1}{1-m}}. \quad (\text{A6})$$

Then, (A1) reads

$$\frac{\dot{\delta}}{\dot{\delta}_0} = D x^{-m}. \quad (\text{A7})$$

Putting (A1) in (4) to eliminate the dependence in $\dot{\delta}$, we obtain

$$\frac{dx}{dt'} = 1 - x^{1-m}, \quad (\text{A8})$$

where $t' = t/T$ with

$$T = \frac{D_c}{D} = \left[\frac{D_c}{\dot{\delta}_0 \theta_0^m} \right]^{1/(1-m)} e^{\frac{x}{B-A}}. \quad (\text{A9})$$

In the sequel, we shall drop the prime and use the dimensionless time t' , meaning that time is expressed in units of T except stated otherwise.

The block sliding behavior is determined by first solving the equation (A8) for the normalized state variable $x(t)$ and then by inserting this solution in (A7) to get the slip velocity. Equation (A8) displays different regimes as a function of m and of the initial value x_i compared to 1 that we now classify.

1.1.1. Case $m = B/A > 1$. For $m > 1$ and $x_i < 1$, the initial rate of change $\frac{dx}{dt}$ of the state variable is negative. The initial decay of x accelerates with time and x reaches 0 in finite time. Expression (A7) shows that $\delta(t)$ continuously accelerates and reaches infinity in finite time. Close to the singularity, we can neglect the first term 1 in the right-hand-side of (A8) and we recover the asymptotic solution (9,10,11):

$$x(t) \simeq m^{\frac{1}{m}} (t_c - t)^{\frac{1}{m}}, \quad (\text{A10})$$

where the critical time t_c is determined by the initial condition $x(t=0) = x_i$

$$t_c = \frac{x_i^m}{m}. \quad (\text{A11})$$

For $m > 1$ and $x_i > 1$, the initial rate of change $\frac{dx}{dt}$ of the state variable is positive, thus x initially increases. This growth goes on, fed by the positive feedback embodied in (A8). At large times, x increases asymptotically at

the constant rate $\frac{dx}{dt} = 1$ leading to $x(t) \approx t$. Integrating equation (A7) gives

$$\delta(t) = \delta_\infty - \frac{\dot{\delta}_0 D}{m-1} \frac{1}{t^{m-1}}, \quad (\text{A12})$$

at large times. The asymptotic value of the displacement δ_∞ is determined by the initial condition. This regime thus describes a decelerating slip slowing down as an inverse power of time. It does not correspond to a destabilizing landslide but to a power law plasticity hardening.

1.1.2. Case $m = B/A = 1$. In this case, the variables (A5) and (A6) are not defined and we go back to (4) (which uses the unnormalized state variable θ and time t) to obtain

$$\frac{d\theta}{dt} = 1 - S\theta_0, \quad (\text{A13})$$

where S is defined by (A2) and depends on the material properties but not on the initial conditions. If $S\theta_0 > 1$, θ decays linearly and reaches 0 in finite time. This retrieves the finite-time singularity, with the slip velocity diverging as $1/(t_c - t)$ corresponding to a logarithmic singularity of the cumulative slip. If $S\theta_0 < 1$, θ increases linearly with time. As a consequence, the slip velocity decays as $\dot{\delta} \sim 1/t$ at large times and the cumulative slip grows asymptotically logarithmically as $\ln t$. This corresponds to a standard plastic hardening behavior.

1.1.3. Case $m = B/A < 1$. For $x_i > 1$, the initial rate of change $\frac{dx}{dt}$ of the state variable is negative, thus x decreases and converges to the stable fixed point $x = 1$ exponentially as

$$x = 1 + ae^{-\frac{t}{t^*}}, \quad (\text{A14})$$

where the relaxation time t^* is given by

$$t^* = \frac{1}{1-m} \quad (\text{A15})$$

in units of T and a is a constant determined by the initial condition. Starting from some initial value, the slip velocity increases for $0 < m < 1$ (respectively decreases for $m < 0$) and converges to a constant, according to (A1,A7).

For $x_i < 1$, the initial rate of change $\frac{dx}{dt}$ of the state variable is positive, and x converges exponentially toward the asymptotic stable fixed point $x = 1$. As θ increases toward a fixed value, this implies that the slip velocity decreases for $0 < m < 1$ (respectively increases for $m < 0$) toward a constant value

Appendix B: Functional renormalization group formulas for the friction law (A7) and (A8)

Consider an expansion as in (13) of an observable $x(t)$ in powers of a variable u given by $x_k(u) = \sum_{n=0}^k a_n u^n$.

The method of algebraic self-similar renormalization constructs so-called “approximants”, which are reconstructed functions that best satisfy the imposed asymptotic constraints while obeying criteria of functional self-similarity and of maximum stability in the space of functions [Yukalov and Gluzman, 1997; Gluzman and Yukalov, 1997; 1998]. These approximants are given by the following general recurrence formula for the approximate $x_k^*(u)$ of order k as a function of the expansion $x_{k-1}(u)$ up to order $k-1$:

$$x_k^*(u) = \left[x_{k-1}^{-k/s}(u) - \frac{k a_k}{s} u^k \right]^{-s/k}. \quad (\text{B1})$$

The crossover index s is determined by the condition that the leading terms of the expansion of $x_k^*(t)$ as $t \rightarrow 0$ must agree with the expansion of $x_k(u)$.

For the friction model (A7) and (A8), the coefficients a_k in (13) and (B1) are determined by the friction parameters and the initial conditions

$$a_0 = y_0, \quad (\text{B2})$$

$$a_1 = \theta_0^{-1} - S y_0^{1-m}, \quad (\text{B3})$$

$$a_2 = \frac{1}{2} S (m-1) a_1 y_0^{-m}, \quad (\text{B4})$$

$$a_3 = \frac{1}{6} \alpha (m-1) [-m a_1^2 y_0^{-m-1} + 2a_2 x_0^{-m}] \quad (\text{B5})$$

$$a_4 = \frac{1}{24} S (m-1) [(1+m) m a_1^3 y_0^{-m-2} - 6m a_2 a_1 y_0^{-m-1} + 6a_3 y_0^{-m}]. \quad (\text{B6})$$

2.1. Case $m < 1$

As we see from (14), the natural expansion variable is $u = \exp(-\frac{t}{t^*})$.

The first-order and simplest approximate is

$$x_1^*(u) = x^* (1+cu)^{-s} = x^* \left(1 + c \exp\left(-\frac{t}{t^*}\right) \right)^{-s}, \quad (\text{B7})$$

with $x^* = 1/T$ where T is given by (A9). The crossover amplitude c and the crossover index s are determined by the condition that the expansion of $x_1^*(t)$ as $t \rightarrow 0$ must agree with the first two terms of expression (13), leading to the following system of equations,

$$x^* (1+c)^{-s} = x_0, \quad (\text{B8})$$

$$x_0 s c \frac{1}{t^*(1+c)} = a_1. \quad (\text{B9})$$

The crossover index s is then given by

$$s = -\frac{\ln(x_0/x^*)}{\ln(1+c)}, \quad (\text{B10})$$

while the crossover amplitude c satisfies the following equation:

$$\frac{\ln(x_0/x^*)}{\ln(1+c)} \frac{c}{(1+c)} = -\frac{a_1 t^*}{x_0}. \quad (\text{B11})$$

The second-order approximate is given by

$$\begin{aligned} x_2^*(u) &= x^* \left[(1+c_2 u)^{-s_2} + c_1 u^2 \right]^{-s_1} \\ &= x^* \left[\left(1 + c_2 \exp\left(-\frac{t}{t^*}\right) \right)^{-s_2} + c_1 \exp\left(-\frac{2t}{t^*}\right) \right]^{-s_1} \end{aligned} \quad (\text{B12})$$

The crossover amplitudes c_1, c_2 and crossover index s_1 and s_2 are obtained from the condition that the expansion of $x_2^*(t)$ as $t \rightarrow 0$ must recover the first four terms of expression (13). The corresponding expressions are rather long and will not be presented here explicitly. Interestingly, for $m = 0$, the second-order approximate recovers the exact solution.

2.2. Case $m \geq 1$

In this case, the natural variable in the expansion is $u = t$. Our goal is to obtain the critical time t_c as a function of m . Using the crossover technique of [Gluzman and Yukalov, 1998] for the two asymptotic expressions (13) at short time and (A10) close to t_c , we obtain a sequence of approximants $x_1^*(t)$, $x_2^*(t)$, $x_3^*(t)$ and $x_4^*(t)$ associated with a sequence of improving approximations for the critical time, $t_{c1}(m)$, $t_{c2}(m)$, $t_{c3}(m)$ and $t_{c4}(m)$. All approximants agree term-by-term with the corresponding short time expansion and lead to the critical behavior (A10) as t goes to the corresponding critical time. The first-order approximate is

$$x_1^*(t) = x_0 \left(1 + \frac{a_1}{x_0} m t \right)^{1/m}, \text{ with } t_{c1} = -\frac{x_0}{m a_1}. \quad (\text{B13})$$

Interestingly, $x_1^*(t)$ coincides with the exact solution in the limit $m \rightarrow \infty$, which takes the form $x = x^* ((x_0/x^*)^m - (t/t^*))^{\frac{1}{m}}$.

In the next order, we obtain the second-order approximate

$$x_2^*(t) = x_0 \left[\left(1 + \frac{a_1}{x_0} t \right)^m + \frac{m a_2}{x_0} t^2 \right]^{1/m}, \quad (\text{B14})$$

and t_{c2} is solution of the following equation

$$\left(1 + \frac{a_1}{x_0} t_{c2} \right)^m + \frac{m a_2}{x_0} t_{c2}^2 = 0. \quad (\text{B15})$$

The third order approximate reads

$$x_3^*(t) = x_0 \left[\left(1 + \frac{a_1}{x_0} t + \frac{a_2}{x_0} t^2 \right)^m + \frac{m a_3}{x_0} t^3 \right]^{1/m}, \quad (\text{B16})$$

and t_{c3} satisfies the following equation

$$\left(1 + \frac{a_1}{x_0} t_{c3} + \frac{a_2}{x_0} t_{c3}^2 \right)^m + \frac{m a_3}{x_0} t_{c3}^3 = 0. \quad (\text{B17})$$

The fourth-order approximate is given by

$$x_4^*(t) = x_0 \left[\left(1 + \frac{a_1}{x_0} t + \frac{a_2}{x_0} t^2 + \frac{a_3}{x_0} t^3 \right)^m + \frac{m a_4}{x_0} t^4 \right]^{1/m}, \quad (\text{B18})$$

with t_{c4} solution of the equation

$$\left(1 + \frac{a_1}{x_0}t_{c4} + \frac{a_2}{x_0}t_{c4}^2 + \frac{a_3}{x_0}t_{c4}^3\right)^m + \frac{m a_4}{x_0}t_{c4}^4 = 0. \quad (\text{B19})$$

Note that for $m = 1$, all approximants are identical and equal to the exact solution.

Appendix C: Functional renormalization of polynomials expansions for the prediction of t_c as a function of the “present time” t_{\max} for La Clapière landslide

This appendix present tests of the prediction of the time at which the velocity peaked, following the hypothesis discussed in the main text that the ensuing deceleration resulted from a change from $x_i < 1$ to $x_i > 1$ in the velocity weakening regime $B > A$. According to this interpretation, the first accelerating phase should be described by an increasing velocity $\propto 1/t_c - t$. The critical time t_c can be approximated by the time of the peak of the velocity, in other words, t_c is close to the inflection point of the displacement as a function of time.

Rather than using the version of the functional renormalization method described for the Vajont landslide based on the slider-block equations of motion, we use here a simpler version that has been tested earlier in another rupture problem [Gluzman *et al.*, 2001]. This choice is governed by the fact that we can not rely entirely on the friction model with fixed parameters since we know that a change of regime occurred. We thus follow a more general approach which is not dependent upon a specialized specification of the equations of motion. The previous investigation on a model system [Gluzman *et al.*, 2001] developed theoretical formulas for the prediction of the singular time of systems which are a priori known to exhibit a critical behavior, based solely on the knowledge of the early time evolution of an observable. From the parameterization of such early time evolution in terms of a low-order polynomial of the time variable, the functional renormalization approach introduced by Yukalov and Gluzman [1997] allows one to transform this polynomial into a function which is asymptotically a power law. The value of the critical time t_c , *conditioned* on the assumption that t_c exists, can then be determined from the knowledge of the coefficients of the polynomials. Gluzman *et al.* [2001] have tested with success this prediction scheme on a specific example and showed that this approach gives more precise and reliable predictions than through the use of the asymptotic power law model, but is probably not better than the true model when the later is known.

The input of the method is the inverse of La Clapière block velocity $\dot{\delta}$ as a function of time up to the “present time” t_{\max} . One starts with a simple polynomial fit of $1/\dot{\delta}$ as a function of time from some starting time up to t_{\max} .

One then applies the functional renormalization method explained in Gluzman *et al.* [2001] to this polynomial expansion. We restrict our analysis to expansions of up to second-order in time:

$$1/\dot{\delta} = 1 + b_1 t + b_2 t^2, \quad (\text{C1})$$

where the zeroth-order coefficient b_0 has been put equal to 1 by a suitable normalization of the data.

The first order approximant for the inverse velocity reads [Gluzman *et al.*, 2001]

$$F_1^*(t) = \left(1 - \frac{b_1}{s_1}t\right)^{-s_1}. \quad (\text{C2})$$

The second order approximant is

$$F_2^*(t) = 1 + b_1 t \left(1 - \frac{b_2}{b_1 s_2}t\right)^{-s_2}. \quad (\text{C3})$$

The exponents s_1 and s_2 are control parameters that are determined from an optimal stability criterion. We follow [Gluzman *et al.*, 2001] and impose $s_1 = s_2 = s$, which is a condition of consistency between the two approximants. s is now the single control parameter, and plays the role of the critical exponent at the critical point t_c . The condition of the existence of a critical point is that both approximants $F_1^*(t)$ and $F_2^*(t)$ of the inverse velocity should vanish at $t = t_c$. This yields two equations determining t_c and s , which can be solved numerically.

The numerical estimates of (t_c, s) depends on the time interval over which the polynomial coefficients b_1 and b_2 are determined. Let t_{\max} denote the last point used in the polynomial fit. Figure 20 shows the numerical estimate of t_c as a function of t_{\max} . More precisely, Figure 20 compares the prediction of a fit using a polynomial of order two in time to the inverse of the velocity (panel (a)) with the prediction of the renormalization approach (panel (b)).

We have also fitted a power law to the data to extract an estimate of t_c as a function of t_{\max} and find an extremely unstable prediction where t_c fluctuates wildly ranging from two years before the end of 1987 to 25 years after 1987. Clearly, predicting the change of regime from a power law fit of the acceleration in the first phase of La Clapière is completely unreliable. In contrast, the renormalized approximants provide a more reasonable stable estimate.

References

Anifrani, J.-C., C. Le Floch, D. Sornette and B. Soulard, Universal Log-periodic correction to renormalization group scaling for rupture stress prediction from acoustic emissions, *J. Phys. I France* 5, 631-638, 1995.
 Bhandari, R. K, Some lessons in the investigation and field monitoring of landslides, *Proceedings 5th Int. Symp. Landslides lausanne 1988*, eds C. Bonnard , 3, 1435-1457, Balkema, 1988.

Blanpied, M. L., D. A. Lockner and J. D. Byerlee, Frictional slip of granite at hydrothermal conditions, *J. Geophys. Res.*, 100, 13045-13064, 1995.

Broili, L., New knowledge on the geomorphology of the Vaiont slide slip surfaces, *Rock mechanics and Engineering*, 5, 38-88, 1967.

Campbell, C.S., Self-lubrification for long runout landslides, *Journal of Geology*, 97, 653-665, 1989.

Campbell, C.S., Rapid granular flow, *Annu. Rev. of Fluid Mech.*, 22, 57-92, 1990.

Caplan-Auerbach, J., C. G. Fox and F. K. Duennebier, Hydroacoustic detection of submarine landslides on Kilauea volcano, *Geophys. Res. Letts.*, 28, 1811-1813, 2001.

David, E. and ATM, Glissement de La Clapière, St Etienne de Tinée, Etude cinématique, géomorphologique et de stabilité, *rapport CETE Nice*, France, 88 pp., 2000.

Davis, R.O., N. R. Smith and G. Salt, Pore fluid frictional heating and stability of creeping landslides, *Int. J. Num. Anal. Meth. Geomechanics*, 14, 427-443, 1990.

Dieterich, J., Time dependent friction and the mechanics of stick slip, *Pure Appl. Geophys.*, 116, 790-806, 1978.

Dieterich, J. H., Earthquake nucleation on faults with rate- and state-dependent strength, *Tectonophysics*, 211, 115-134, 1992.

Durville, J.L., Study of mechanisms and modeling of large slope movements, *Bull. Int. Ass. Engineering Geology*, 45, 25-42, 1992.

Eisbacher, G.H., Cliff collapse and rock avalanches in the Mackenzie Mountains, Northwestern Canada, *Can. Geot. J.*, 16, 309-334, 1979.

Erismann, T.H. and G. Abele, *Dynamics of Rockslides and Rockfalls*, Springer, 300 pp, 2000.

Follacci, J. P., Photographic album of La Clapière landslide, *CETE Méditerranée*, 2000.

Follacci, J. P., P. Guardia and J. P. Ivaldi, La Clapière landslide in its geodynamical setting, *Bonnard eds*, Proc. 5th Int. Symp. on Landslides, 3, 1323-1327, 1988.

Follacci, J.-P., L. Rochet and J.-F. Serratrice, Glissement de La Clapière, St Etienne de Tinée, Synthèse des connaissances et actualisation des risques, *rapport 92/PP/UN/I/DRM/03/AI/01*, Ministère Environnement, 76 pp., 1993.

Fruneau, B., J. Achache and C. Delacourt, Observation and modeling of the Saint-Etienne-de-Tinée landslide using SAR interferometry, *Tectonophysics*, 265, 181-190, 1996.

Fukuzono, T., Method for predicting the failure time of a slope, *Proceedings of the 4th Int. Conf. Field Workshop on Landslides*, National Research Center for Disaster prevention, Tokyo, 145-150, 1985.

Gluzman, S. and V. I. Yukalov, Algebraic self-similar renormalization in the theory of critical phenomena, *Phys. Rev. E*, 55, 3983-3999, 1997.

Gluzman, S. and V. I. Yukalov, Unified approach to crossover phenomena, *Phys. Rev. E*, 58, 4197-4209, 1998.

Gluzman, S. and D. Sornette, Self-Consistent theory of rupture by progressive diffuse damage, *Physical Review E*, 6, 306 N6 PT2:6129,U241-U250, 2001.

Gluzman, S. and D. Sornette, Classification of possible finite-time singularities by functional renormalization, in press in *Phys. Rev. E*, 2002 (<http://arXiv.org/abs/cond-mat/0111181>).

Gluzman, S., J. V. Andersen and D. Sornette, Functional Renormalization Prediction of Rupture, *Computational Seismology*, 32, 122-137, 2001.

Gomberg, J., P. Bodin, W. Savage and M. E. Jackson, Landslide faults and tectonic faults, Analogs? – The slumgullion earthflow, Colorado, *Geology*, 23, 41-44, 1995.

Gomberg, J., N. Beeler and M. Blanpied, On rate-state and Coulomb failure models, *J. Geophys. Res.*, 105, 7857-7871, 2000.

Guglielmi, J., and J. M. Venegeon, Interrelation between gravitational patterns and structural fractures La Clapière, French Alps, submitted to *Geomorphology*, 2002.

Heim A., *Bergsturz und Menschenleben*, Zurich, 1932.

Hendron, A. J. and F. D. Patton, The Vaiont slide, a geotechnical analysis based on new geologic observations of the failure surface, *US Army Corps of Engineers Technical Report GL-85-5 (2 volumes)*, 1985.

Huang, Y., A. Johansen, M. W. Lee, H. Saleur and D. Sornette, Artifactual Log-Periodicity in Finite-Size Data: Relevance for Earthquake Aftershocks, *J. Geophys. Res.*, 105, 25451-25471, 2000.

Hoek, E. and E. T. Brown, *Undergrond excavation in rock*, Institution of Mining and Metallurgy, London, 1980.

Hoek, E., and J. W. Bray, *Rock slope engineering*, 3rd Edn (rev), Institution of Mining and Metallurgy and E&FN Spon, London, pp 358, 1997.

Jaume, S. C. and L. R. Sykes, Evolving toward a critical point: A review of accelerating seismic moment/energy release prior to large and great earthquakes, *Pure and Appl. Geophys.*, 155, 279-305, 1999.

Kennedy B. A. and K. E. Niermeyer, Slope Monitoring systems used in the Prediction of a Major Slope Failure at the Chuquicamata Mine, Chile, *Proc. on Planning Open Pit Mines, Johannesburg*, Balkema, 215-225, 1971.

Kilburn, C. R. J., and D. N. Petley, Forecasting giant, catastrophic slope collapse: lessons from Vajont, Northern Italy, in press. *Geomorphology*, 2002.

Korner, H. J., Reichweite und Geschwindigkeit von Bergsturzen und Fleisscheneelawinen, *Rock mechanics*, 8, 2256-256, 1976.

Malet, J. P., O. Maquaire and E. Calais, The use of Global Positioning System techniques for the continuous monitoring of landslides: application to the Super-Sauze earthflow (Alpes-de-Haute-Provence, France), *Geomor-*

phology, 43, 33-54, 2002.

Mantovani, F., R. Soeters and C. J. Vanwesten, Remote sensing techniques for landslide studies and hazard zonation in Europe, *Geomorphology*, 15, 213-225, 1996.

Marone, C., Laboratory-derived friction laws and their application to seismic faulting, *Ann. Rev. Earth Planet. Sci.*, 26, 643-696, 1998.

Muller L., The rock slide in the Vajont valley, *Felsmechanik und Ingenieurgeologie*, 2 (3-4), 148-212, 1964.

Muller L., News consideration on the Vajont slide, *Felsmechanik und Ingenieurgeologie*, 6, 1-91, 1968.

Parise, M., Landslide mapping techniques and their use in the assessment of the landslide hazard, *Phys. Chem. Earth, Part C- Solar-Terr. Plan. Sci.*, 26, 697-703, 2001.

Pisarenko V.F., A. A. Lyubushin, S. Canu, M. F. Kanevsky, E. A. Savelieva, V. V. Demianov, M. V. Bolgov, T. A. Rukavishnikova, and I. V. Zalyapin, Statistical methods for river's runoff forecast, 2002, submitted to *Water Resources Research*. (this paper was presented at the 4-th INTAS Interdisciplinary Symposium on Physical and Chemical Methods in Biology, Medicine and Environment, Moscow, May 30 - June 3, 2001).

Rabotnov, Y. N., *Creep problems in Structural Members*, North-Holland eds, Amsterdam, 1969.

Rat, M., Difficulties in foreseeing failure in landslides - La Clapière, French Alps, *Proceedings 5th Int. Symp. Landslides lausanne 1988*, eds C. Bonnard, vol 3, 1503-1504, Balkema, 1988.

Rousseau, N., Study of seismic signals associated with rockfalls at 2 sites on the Reunion island (Mahavel Cascade and Soufrière cavity), *PhD thesis*, IPG Paris, 1999.

Ruina, A. L., Slip instability and rate variable friction laws, *J. Geophys. Res.*, 88, 10359-10370, 1983.

Saito, M., Forecasting the Time of occurrence of a Slope Failure, *Proc. 6th Int. Conf. Soil Mech. & Found. Eng.*, Montreal, vol.2, 537-541, 1965.

Saito, M., Forecasting time of Slope Failure by Tertiary Creep, *Proc. of 7th Int. Conf. Soil Mech. & Found. Eng.*, Mexico City, vol. 2, 677-683, 1969.

Saito, M. and H. Uezawa, Failure of soil due to creep, *Proc. of 6th Int. Conf. Soil Mech. & Found. Eng.*, Montreal, vol. 1, 315-318, 1961.

Sammis, S. G. and D. Sornette, Positive Feedback, Memory and the Predictability of Earthquakes, *Proceedings of the National Academy of Sciences USA*, 99, 2501-2508, 2002.

Scholz, C. H., The mechanics of earthquakes and faulting Cambridge University Press, 1990.

Scholz, C. H., Earthquakes and friction laws, *Nature*, 391, 37-42, 1998.

Smith, L.A., C. Ziehmann and K. Fraedrich, Uncertainty dynamics and predictability in chaotic systems, *Quarterly J. Royal Meteor. Soc.*, 125, 2855-2886, 1999.

Sornette, D., Predictability of catastrophic events: material rupture, earthquakes, turbulence, financial crashes and human birth, *Proceedings of the National Academy of Sciences USA*, 99, 2522-2529, 2002.

Sornette, D. and C. G. Sammis, Complex critical exponents from renormalization group theory of earthquakes: Implications for earthquake predictions, *J. Phys. I France*, 5, 607-619, 1995.

Sornette, D. and A. Johansen, Significance of log-periodic precursors to financial crashes, *Quantitative Finance* 1, 452-471, 2001.

Susella, G. and F. Zanolini, Risques générés par les grands mouvements de terrains, eds, *Programme Interreg 1, France-Italie*, 207 pp., 1996.

Van Asch, T. W. J., J. Buma and L. P. H. Van Beek, A view on some hydrological triggering systems in landslides, *Geomorphology*, 30, 25-32, 1999.

Vangenuchten, P. M. B. and H. Derijke, Pore water pressure variations causing slide velocities and accelerations observed in a seasonally active landslide, *Earth Surface Processes and Landforms*, 14, 577-586, 1989.

Vere-Jones, D., R. Robinson and W. Z. Yang, Remarks on the accelerated moment release model: problems of model formulation, simulation and estimation, *Geophys. J. Int.*, 144, 517-531, 2001.

Vibert C., M. Arnould, R. Cojean, J. M. Cleac'h, An attempt to predict the failure of a mountainous slope at St Etienne de Tinée, France, *Proceedings 5th Int. Symp. Landslides lausanne 1988*, eds C. Bonnard, vol 2, 789-792, Balkema, 1988.

Voight, B. eds, 2, *Engg. Sites, Development in Geotech. Engg.*, vol. 14b, 595-632, 1978.

Voight, B., A method for prediction of Volcanic Eruption, *Nature*, 332, 125-130, 1988.

Voight, B. A., A relation to describe rate-dependent material failure, *Science*, 243, 200-203, 1989.

Voight B., Materials science laws applies to time forecast of slope failure, *Proceedings 5th Int. Symp. Landslides lausanne 1988*, eds C. Bonnard, vol 3, 1471-1472, Balkema, 1988.

Xu Z. Y., S. Y. Schwartz and T. Lay, Seismic wave-field observations at a dense small-aperture array located on a landslide in the Santa Cruz Mountains, California, *Bull. Seis. Soc. Am.*, 86, 655-669, 1996.

Yukalov, V. I. and S. Gluzman, Self-similar bootstrap of divergent series, *Phys. Rev. E*, 55, 6552-6565, 1997.

Yukalov V.I. and S. Gluzman, Weighted fixed points in self-similar Analysis of Time Series, *International Journal of Modern Physics B*, 13, 1463-1476, 1999.

Ziehmann, C., L. A. Smith and J. Kurths, Localized Lyapunov exponents and the prediction of predictability, *Phys. Lett. A*, 271, 237-251, 2000.

Agnès Helmstetter, Laboratoire de Géophysique Interne et Tectonophysique, Observatoire de Grenoble, Université Joseph Fourier, BP 53X, 38041 Grenoble Cedex, France. (e-mail: ahelmste@obs.ujf-grenoble.fr)

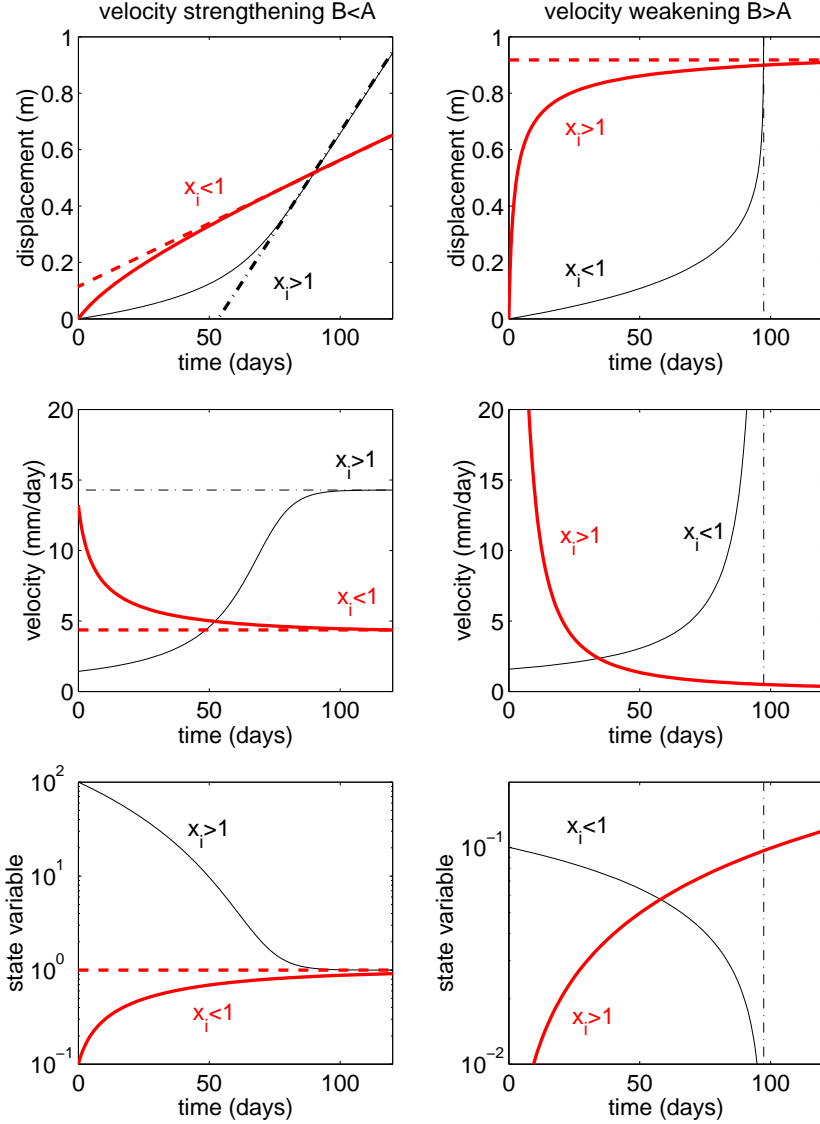


Figure 1. Schematic classification of the different regimes of sliding discussed in the text. The left column of three panels correspond to the stable regime $m = B/A < 1$ and the right column of three panels describes the unstable regime $m = B/A > 1$. In each case, the displacement, velocity and state variables are shown as a function of time. Each regime (stable and unstable) are divided into two cases, depending on the dimensionless initial value $x_i \propto \theta_i$ of the state variable. The thick lines corresponds to decreasing velocities and increasing state variables. The thin lines correspond to increasing velocities and decreasing state variables.

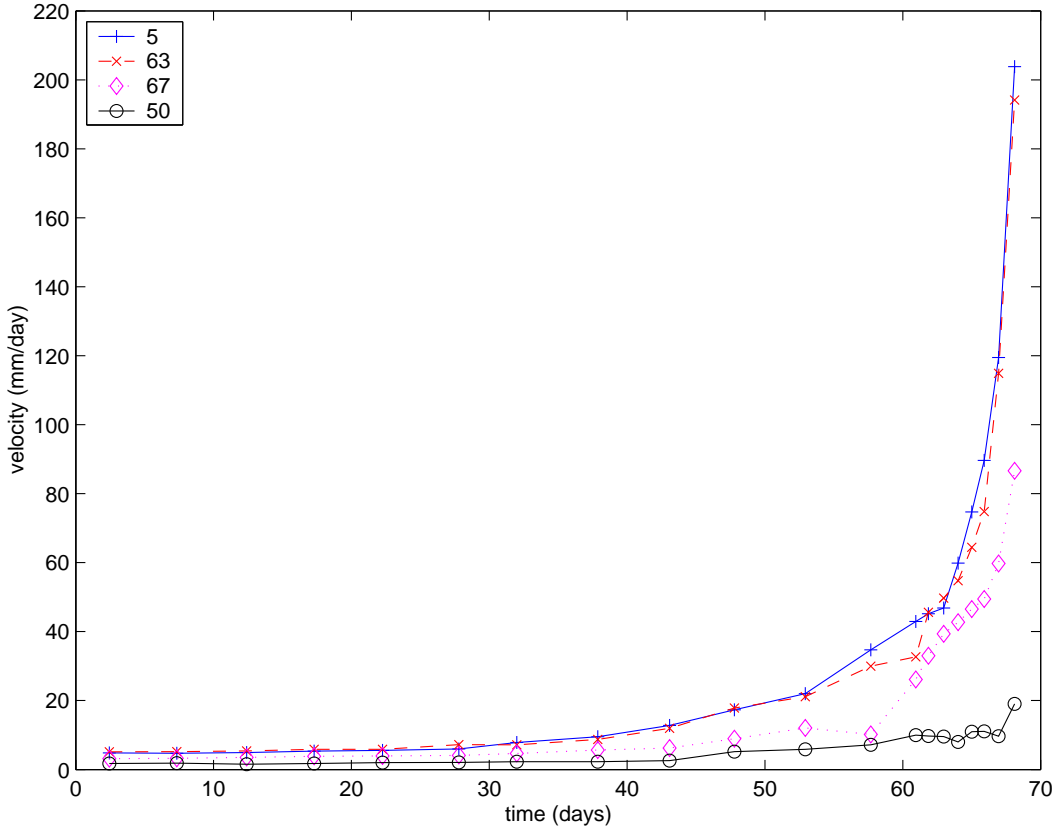


Figure 2. Velocity measurements for the four benchmarks of the Vajont landslide. Benchmarks 5 and 63 exhibit almost the same strong acceleration. Benchmark 50 is the only one which shows only a relatively small acceleration in absolute values at the end of the 60 days accelerating phase. Its acceleration is however significant in relative values, as seen in Figure 4. Data from [Muller, 1964].

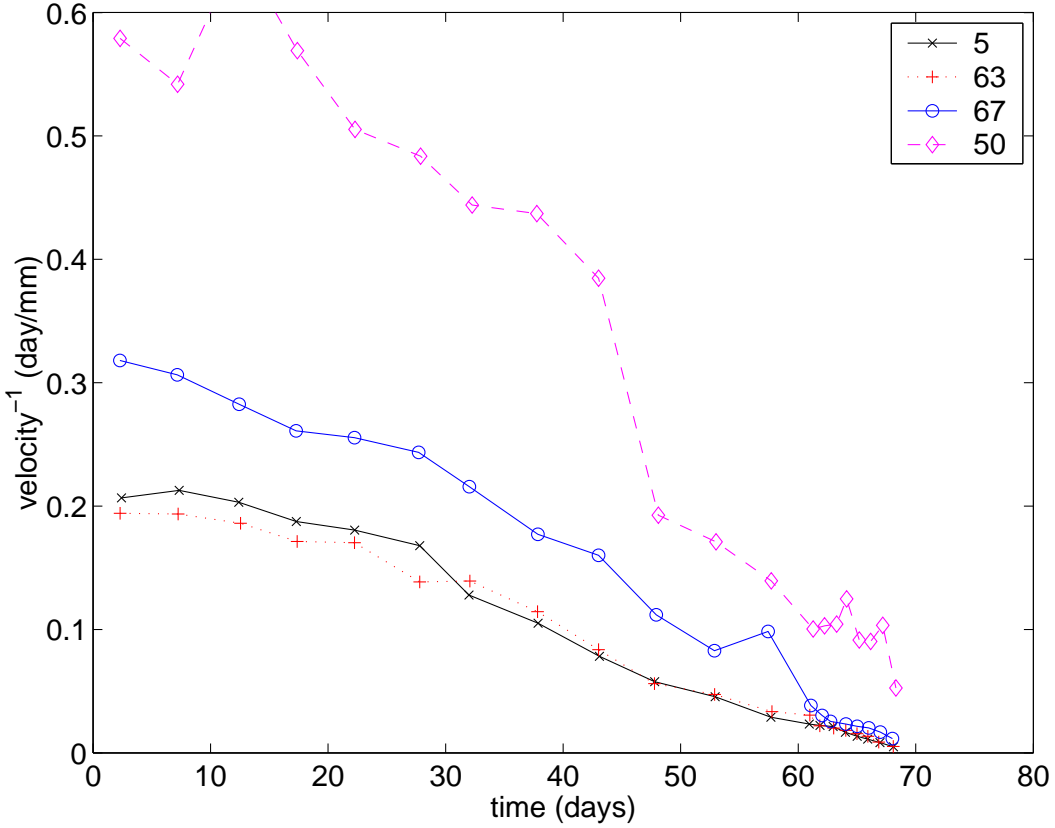


Figure 3. Same as Figure 2 by plotting the inverse of the velocity as a time t . All curves are approximately linear, showing that the velocity exhibits a finite-time singularity $v \sim 1/(t_c - t)$ with $t_c \approx 69.5$ days for all benchmarks, estimated as the intercept of the extrapolation of these curves with the horizontal axis.

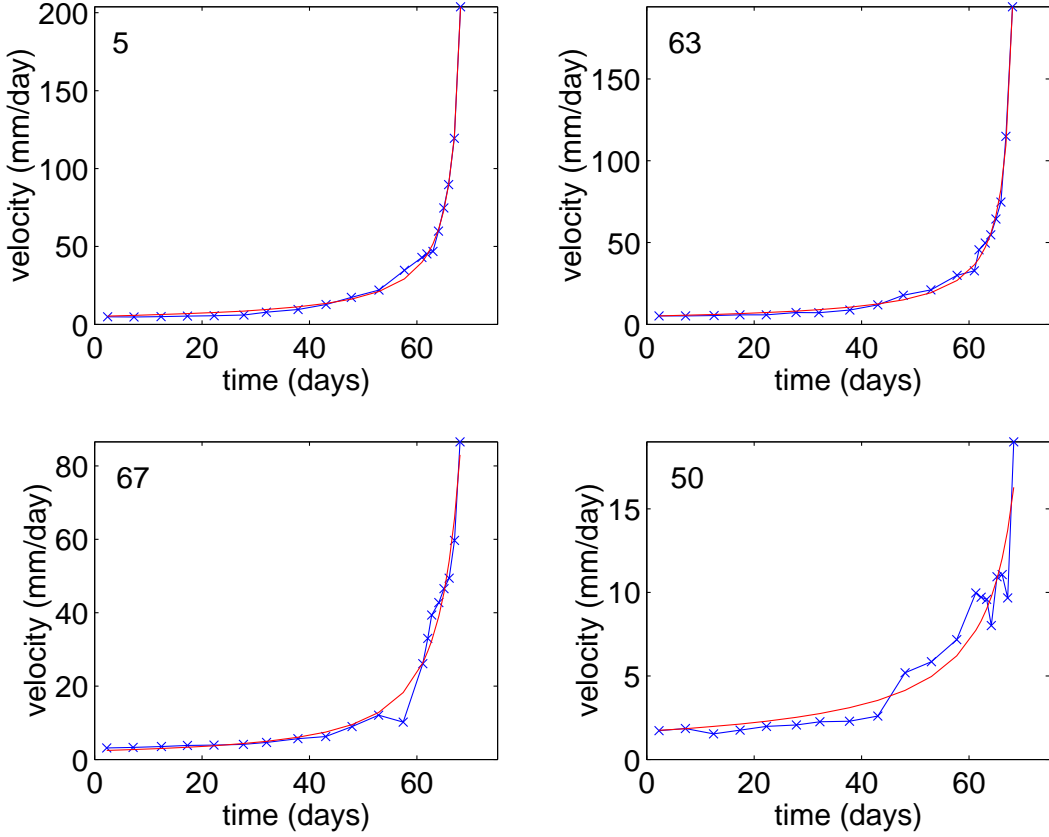


Figure 4. For each of the four Vajont benchmarks, the velocity data of Figure 2 is fitted with the slider-block model with the state and velocity friction law (A8) and (A7) by adjusting the set of parameters m , D , T and the initial condition of the state variable x_i . The data is shown as the crosses linked by straight segments and the fit is the thin continuous line. The fitted m are respectively $m = 1.35$ (benchmark 5), $m = 1.24$ (benchmark 63), $m = 0.99$ (benchmark 67) and $m = 1.00$ (benchmark 50).

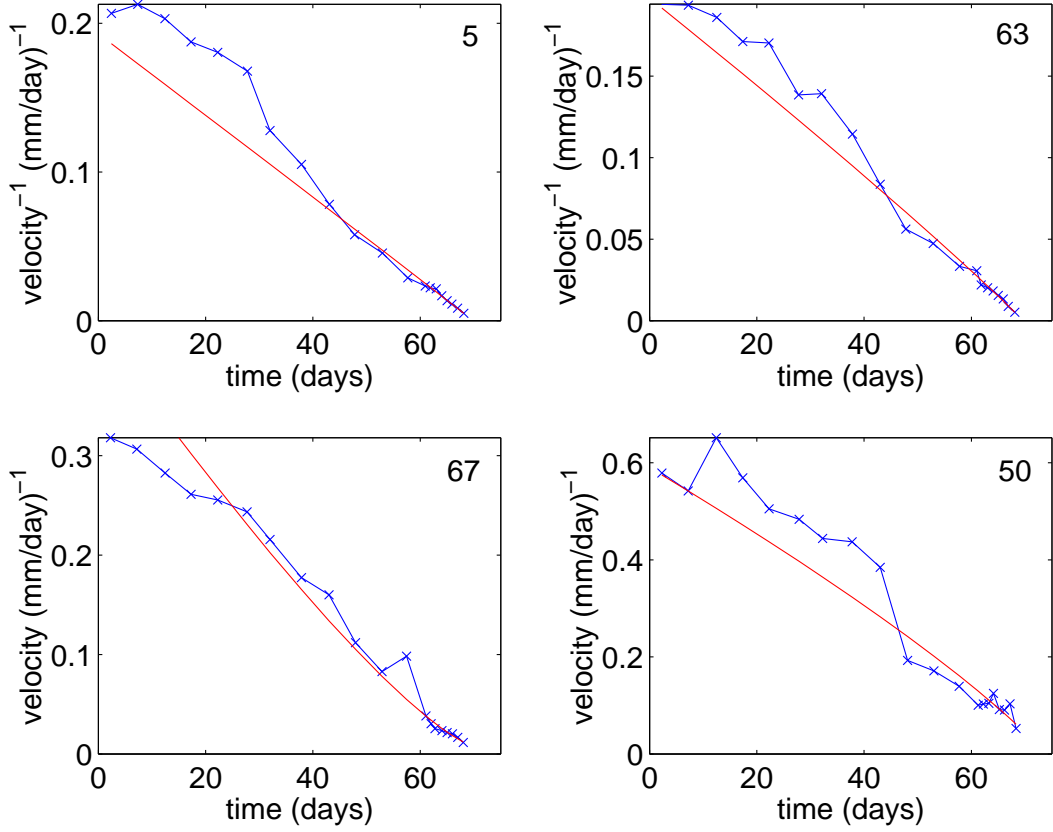


Figure 5. Same as Figure 4 but showing the inverse of the velocity. The upward bending of the curve for benchmark 67 reflects the saturation of the velocity in the stable regime $B < A$. The fit for the three other benchmarks characterized by $m \geq 1$ is very close to the asymptotic solution $v \sim 1/(t_c - t)$ (11).

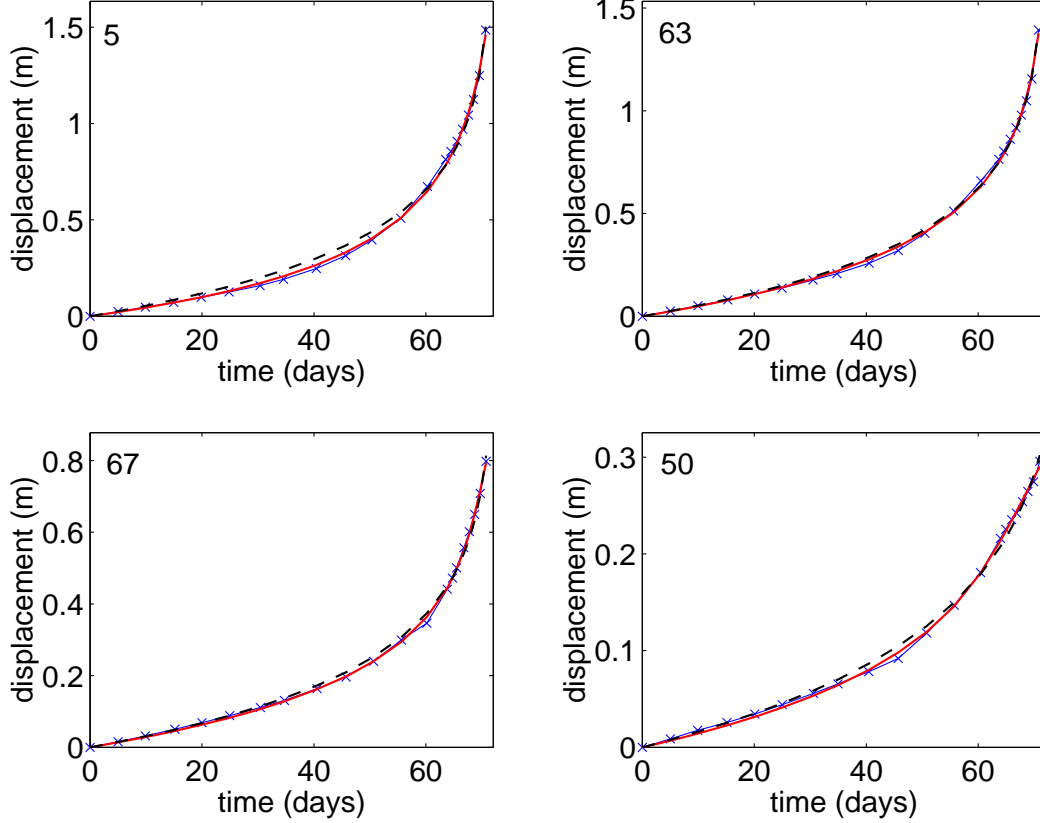


Figure 6. For each of the four Vajont benchmarks, the cumulative displacement data is fitted with the slider-block model with the state and velocity friction law (A8) and (A7) by adjusting the set of parameters m , D/T and the initial condition of the state variable x_i . The data is shown as the crosses linked by straight segments and the fit is the thin continuous line. The fitted m are respectively $m = 0.99$ (benchmark 5), $m = 0.85$ (benchmark 63), $m = 0.68$ (benchmark 67) and $m = 0.17$ (benchmark 50). The fits with the slider-block model obtained by imposing the value $m = 1.5$ are shown with the dashed line for comparison.

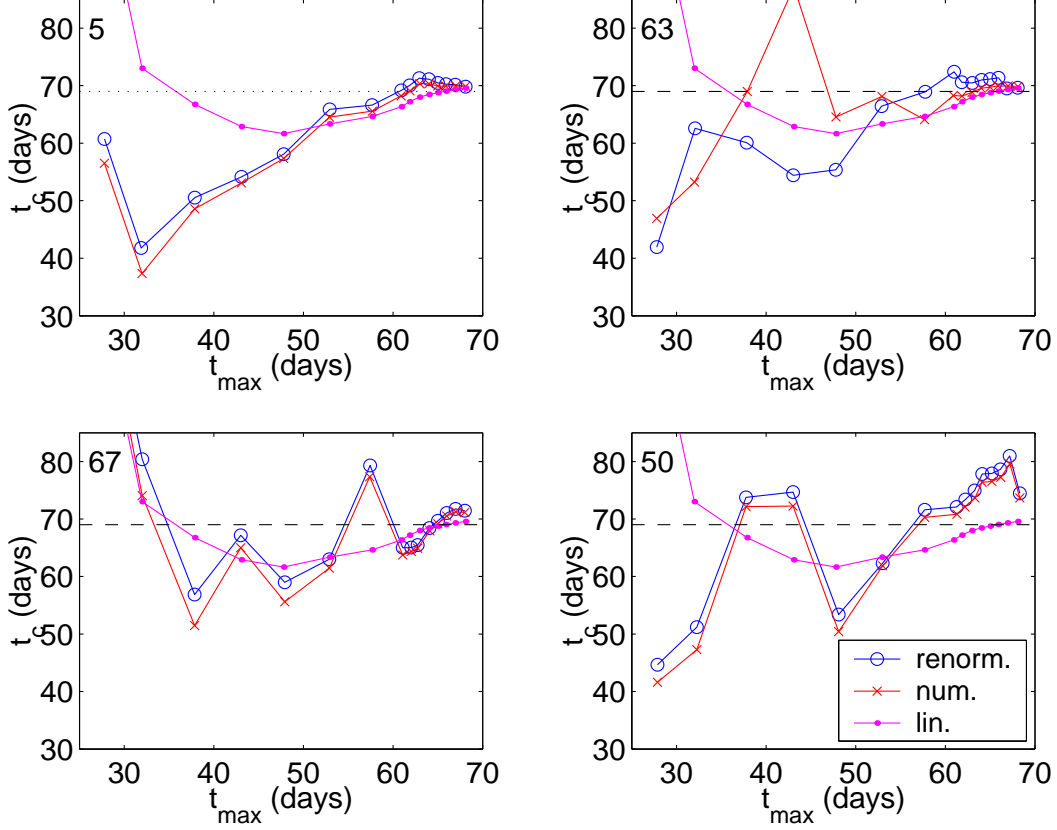


Figure 7. Predicted critical time t_c as a function of the “present time” t_{max} (last point used for the fit) for all four benchmarks of the Vajont landslide, using three different methods of prediction described in the text: renormalization method (circles), numerical evaluation of the friction model (A8) (crosses), and linear regression of the inverse velocity as a function of time performed by removing the first point (early time) of the curve and using a weight proportional to the velocity (dots). The horizontal dashed line indicated the true critical time $t_c = 69.5$ days (for an arbitrary origin of time from which the fits are performed to the catastrophic landslide. All methods impose $m > 1$, but in some cases a better fit may be obtained in the stable regime $m < 1$.

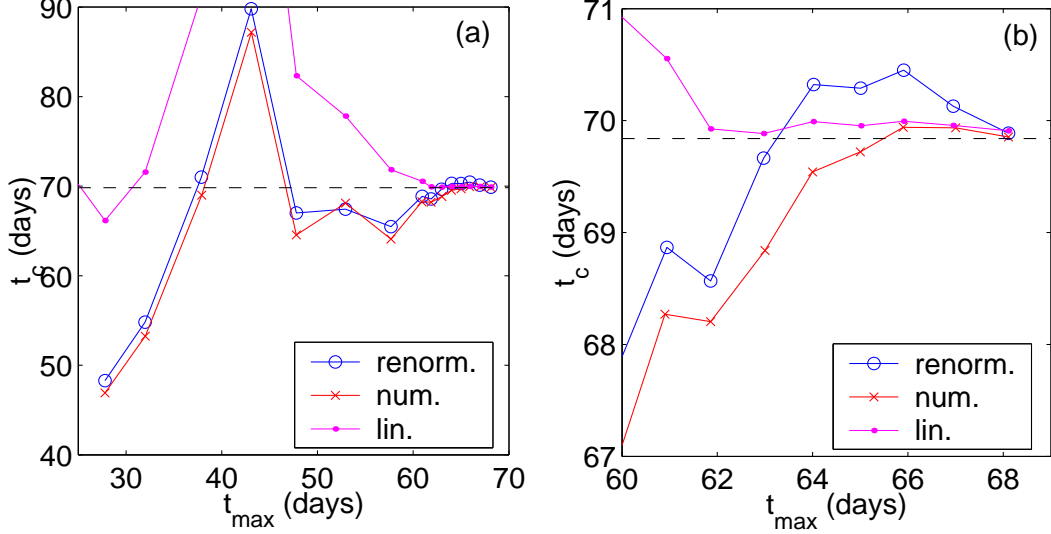


Figure 8. Same as Figure 7 for a synthetic data set with the same parameters and noise as those obtained for benchmark 5 of the Vajont landslide, using the same three different methods of prediction. The right panel is a zoom of the left panel close to t_c . The horizontal dashed line indicated the true critical time $t_c = 69.8$ of the catastrophic landslide.

Figure 9. a) Picture of La Clapière landslide taken in 1979. It is located at an elevation between 1100 m and 1800 m on a slope that culminates at 3000 m high and has a width of about 1000 m. The summit of the main scarp ranges in elevation between 1550 and 1735 m. The volume of mostly gneiss rocks implied in the landslide is estimated to be around 50×10^6 m³. The summit scarp are not connected. b) Picture of La Clapière landslide taken in 1999. Geomorphological criteria allow one to distinguish three distinct sub-entities within the landslide, NW, Central and SW respectively [Follacci *et al.*, 1988]. The global surfacial pattern is preserved. The main feature related to the 1982-1988 crisis is a new summit scarp with a total displacement of about 100 m in 1999, indicated by an arrow in panel (b).

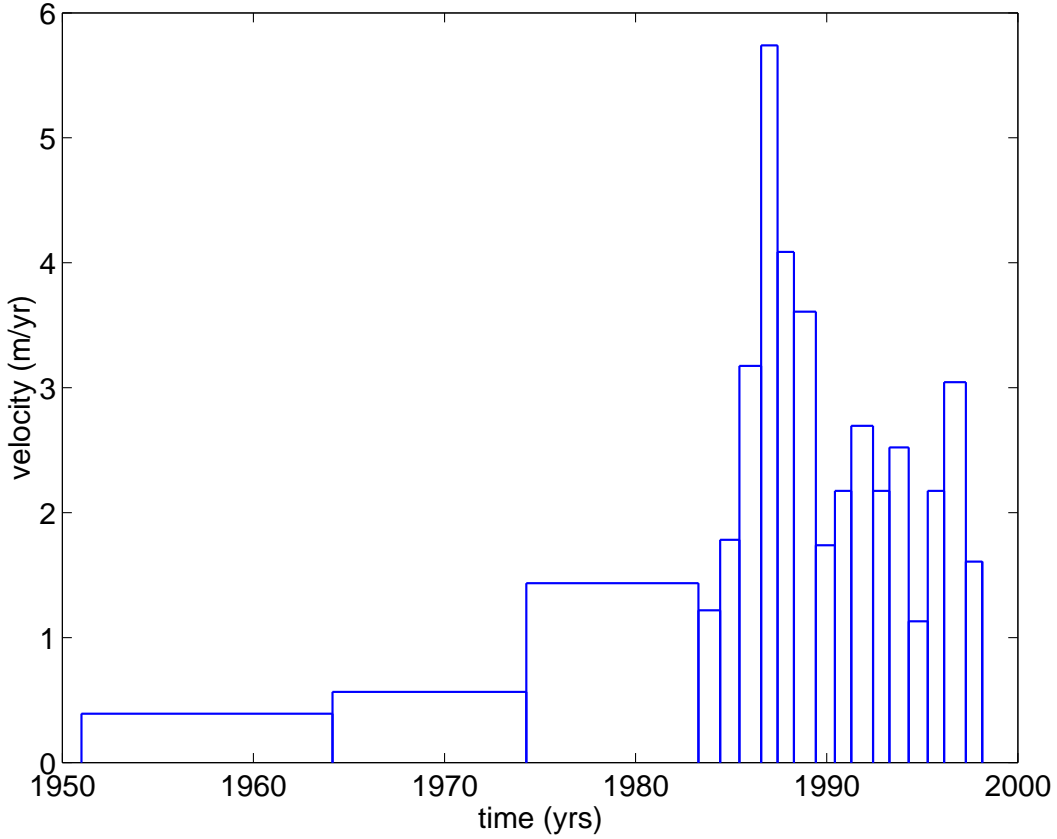


Figure 10. Velocity in meters/year of the side of La Clapière mount over almost 50 years, showing that the dangerous velocity peak in 1987 was preceded by a progressing build-up extending over several decades. Before 1982, the velocity is inferred from aerial photographs in 1951, 1964, 1974 and 1982. After 1982, the velocity is obtained from automated triangulation and geodesy. Data from *CETE* [1999].

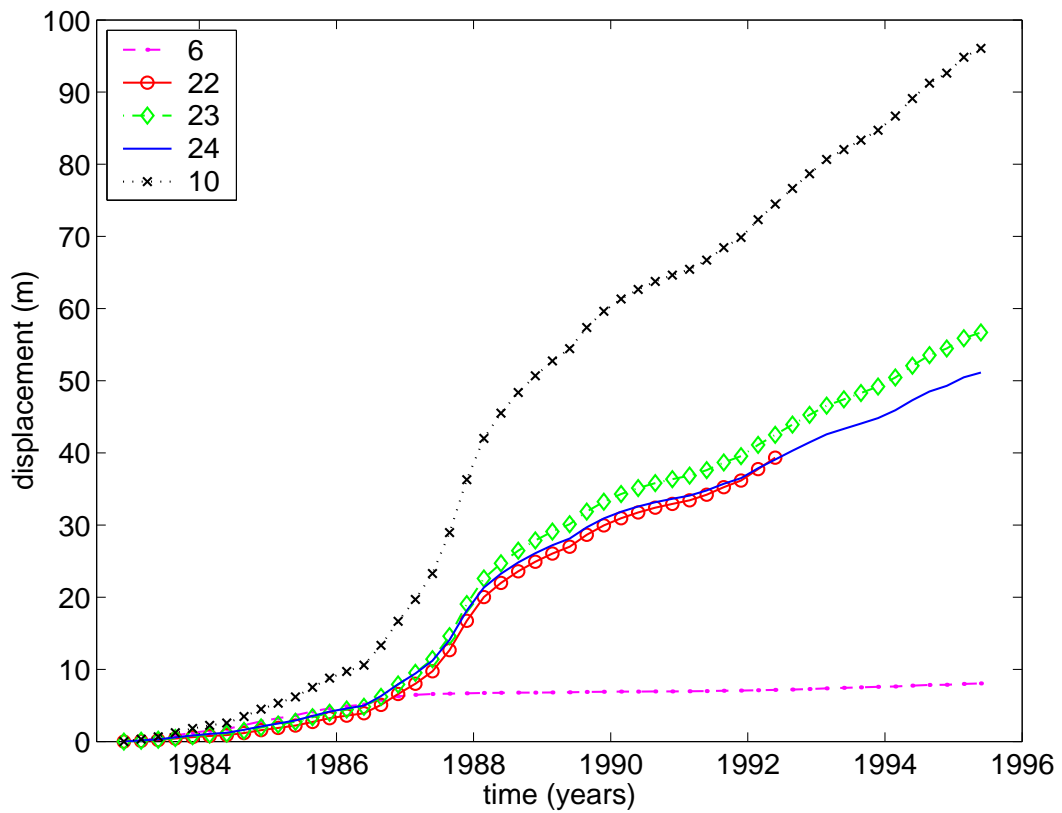


Figure 11. Displacement for the 5 benchmarks on La Clapière site shown in Figure 9.

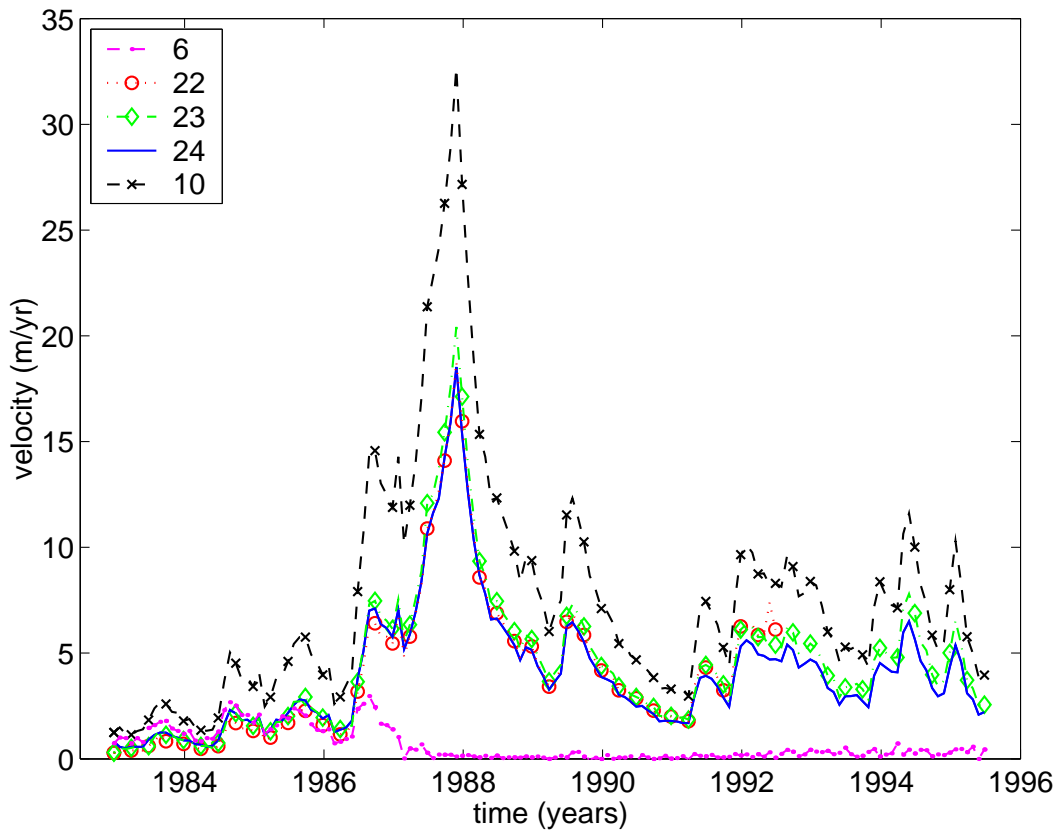


Figure 12. Velocity for the same data as shown in Figure 11. Annual fluctuations of the velocity is due to the seasonal variations of the precipitations.

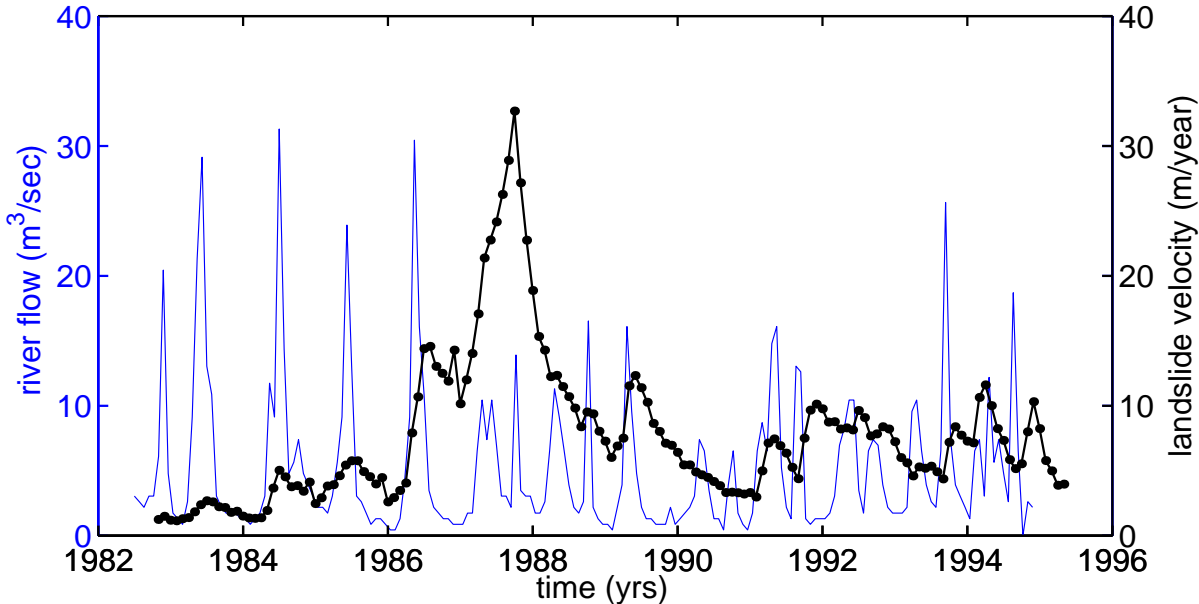


Figure 13. Velocity pattern for benchmark 10 of La Clapière landslide (solid line and dots) and flow rates (thin solid line) of the Tinée river on the 1982-1995 period. Because the Tinée river runs at the basis of the La Clapière landslide, the river flow rate reflects the water flow within the landslide [Follacci *et al.*, 1993; Susella and Zanolini, 1996]. The flow rates are measured at St Etienne village, 2 km upstream the landslide site. There is no stream network on the landslide site. The Tinée flow drains a 170 km^2 basin. This tiny basin is homogeneous both in terms of slopes and elevation (in the 1000-3000 m range). Accordingly the seasonal fluctuations of the river flow is admitted to reflect the evolution of the amount of water that is available within the landslide slope due to rainfalls and snow melting. Data from CETE, [1996].

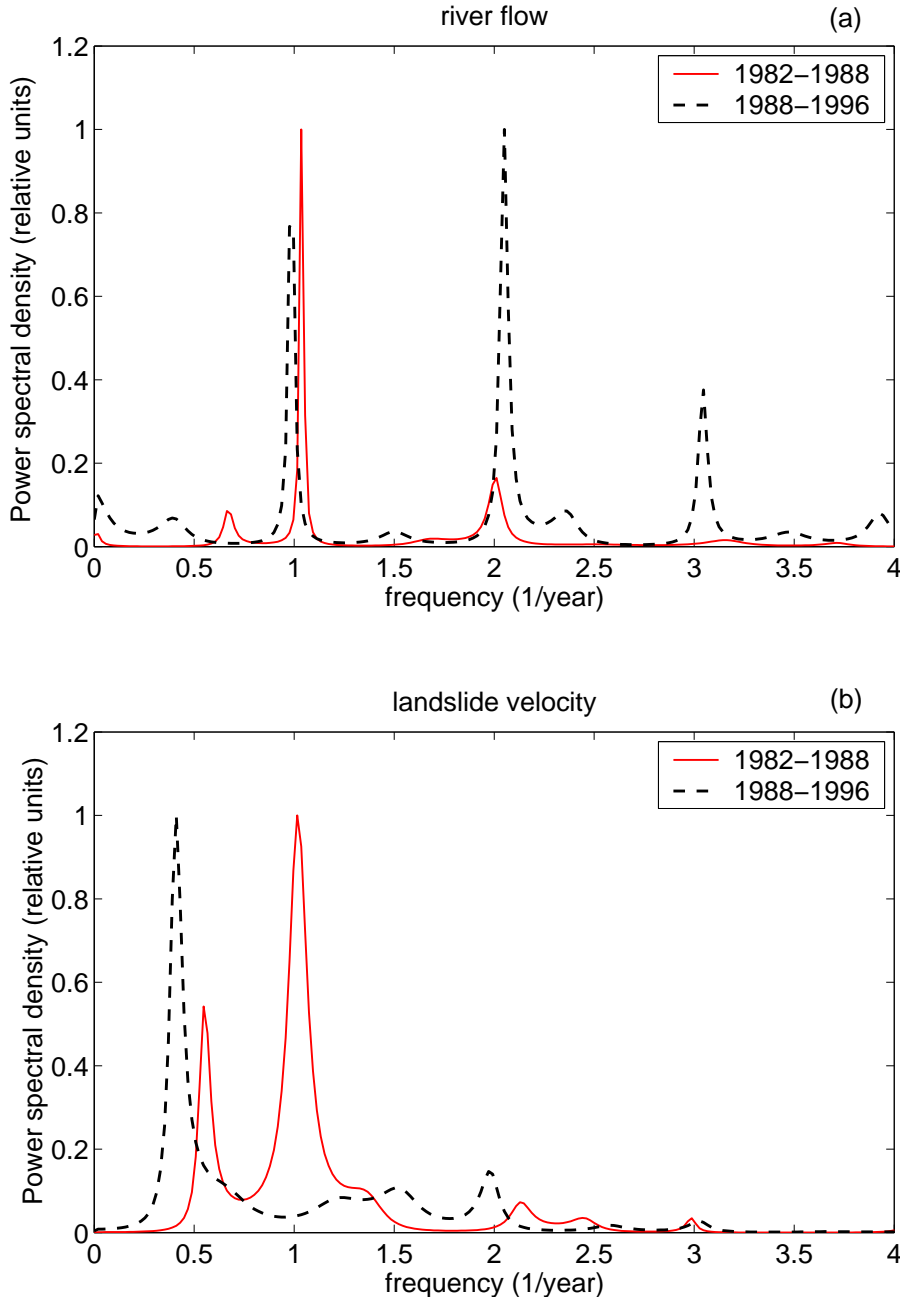


Figure 14. top panel: Burg's power spectrum of the flow rates of the Tinée river on the 1982–1988 and on the 1988–1996 periods which are aggregated from the periods shown in figure 13. Bottom panel: Burg's power spectrum of the detrended velocity residuals for the same two periods.

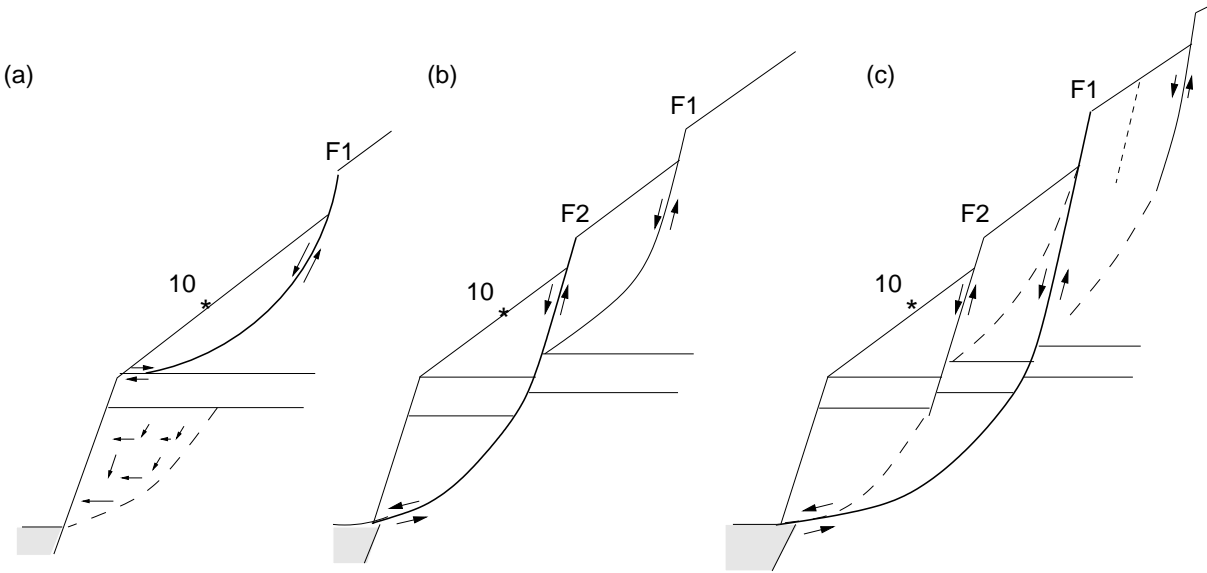


Figure 15. Schematic structural interpretation of one possible mechanism involved in the 1986-1988 crisis. The 3 schematic cross sections are the proposed landslide geometries, before 1986 (a), during the 1987 acceleration (b), and after 1988 (c). *Follacci et al. [1993]* argue for the failure of the strong gneiss bed (F2 fault) in the NW block as the driving force behind the 1986-1987 accelerating phase (b). In the same period, the development of the upper NW crack, (F1 fault on central cross section), that released the landslide from its head driving force, appears as the key parameter to slow down the accelerating slide. Note that for the global landslide structural pattern. *Guglielmi and Vengeon. [2002]* argue for all the surface faulting patterns to converge at shallow depth as listric faults that define a decollement level which is the sliding surface. The arrow shows the location of benchmark 10 (adapted from [Follacci et al., 1993]).

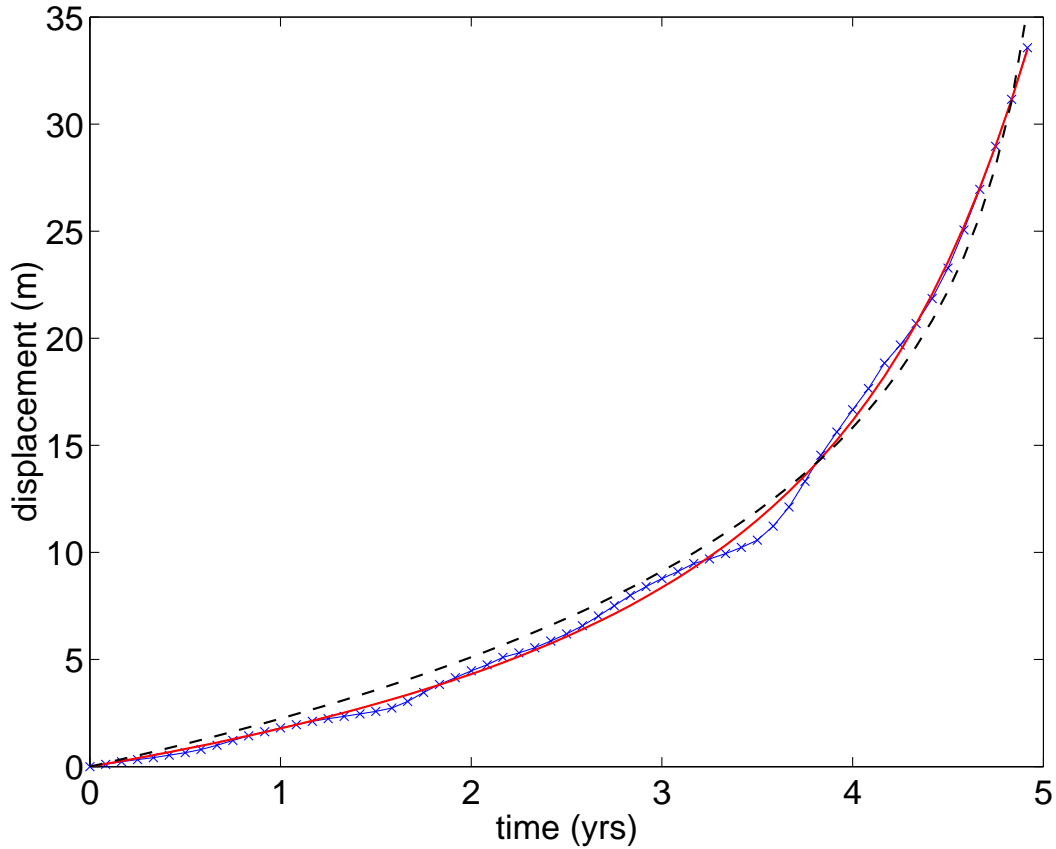


Figure 16. Displacement for benchmark 10 of la Clapière landslide (crosses) and fit using the friction model. The best fit gives $m = 0.98$ (black line). The gray line shows the best fit obtained when imposing $m = 1.5$ for comparison.

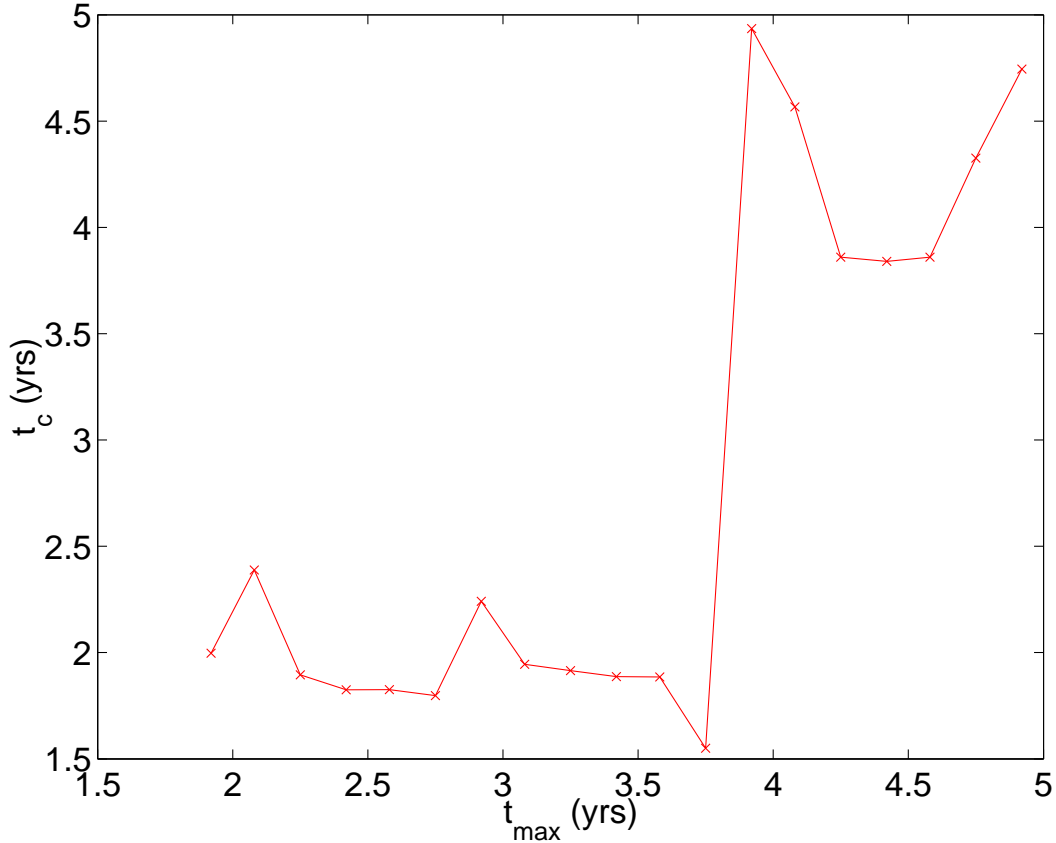


Figure 17. Predicted value of the time t_c of the inflection point of the velocity for La Clapière landslide, using a fit of the displacement data with the friction model. All points correspond to the stable regime $m < 1$. In this regime there is no finite-time singularity of the velocity but a transition from an accelerating sliding to a stable sliding for times larger than the inflection point t_c . This parameter is poorly constrained by the fit and increases with the time of the last point t_{max} used in the fit.

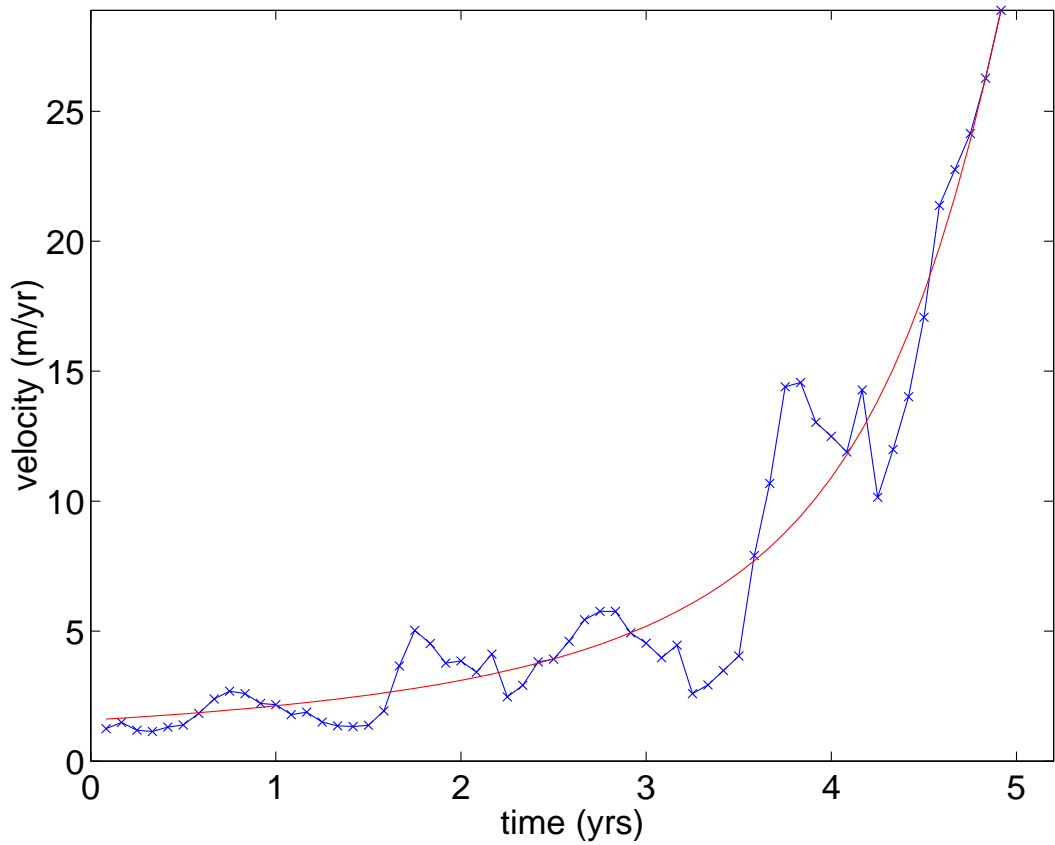


Figure 18. Velocity for benchmark 10 of la Clapière landslide (crosses) and fit of the velocity data with the friction model. The best fit gives $m = 0.99$ (black line).

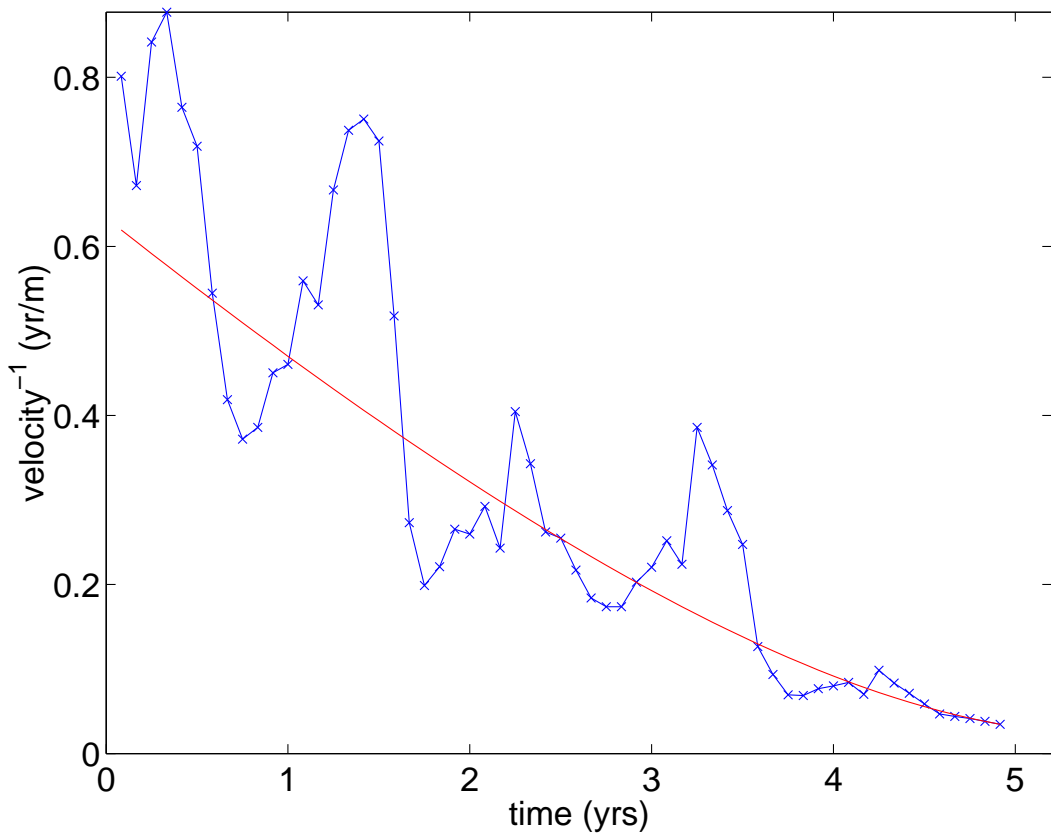


Figure 19. Same as Figure 18 showing the inverse of the velocity.

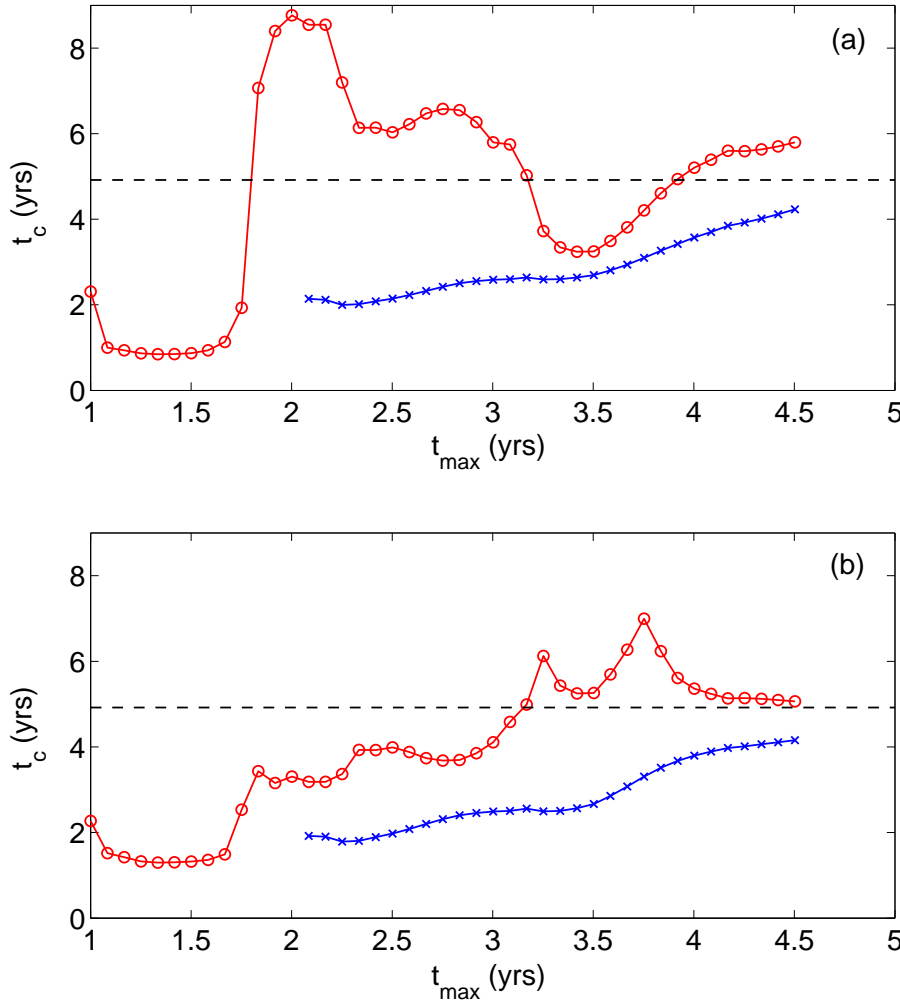


Figure 20. Panel (a): prediction of a critical time using a fit with a polynomial of order two in time to the inverse of the velocity; panel (b): prediction of the renormalization approach described in Appendix C. In each panel, two curves are presented corresponding to two different starting points of the data taken into account in the predictions: the leftmost points correspond to the first date taken into account in the predictions; the predictions corresponding to the crosses \times use approximately two years fewer data than the predictions shown with the open circles. The abscissa t_{max} is the running “present time”, that is, the last time of the data taken into account to issue a prediction. The maximum realized velocity occurred at a time indicated by the horizontal dashed line. This time is thus a proxy for the ghost-like critical time of the landslide.

Table 1. Synthesis of the different regimes of slip as a function of $m = B/A$ (by definition (A3)), of the initial condition x_i on θ and of the material parameter S . A and B are defined in (3) and are determined by material properties. x_i is the initial value of the reduced state variable θ defined in (A5). FTS stands for “finite-time singularity.” The parenthesis (x_i) and (S) in the first column indicates which is the control parameter determining the nature of the slip. The parameter S is defined by (A2) and is independent of the initial conditions. While A is always found positive in laboratory experiments, negative B -values are sometimes found [Blanpied *et al.*, 1995] leading to the possibility of having $m < 0$: this rather special case corresponds to a friction coefficient decreasing with the increase of the surface of contacts.

	$x_i, S < 1$	$x_i, S > 1$
$m > 1 (x_i)$	FTS (9,10,11)	power law plasticity hardening (A12)
$m = 1 (S)$	$\dot{\delta} \sim 1/t$ and $\delta \sim \ln t$	FTS (9,10,11)
$0 < m < 1 (x_i)$	$\theta \downarrow \text{const}$, $\dot{\delta} \uparrow \text{const}$	$\theta \uparrow \text{const}$, $\dot{\delta} \downarrow \text{const}$
$m < 0 (x_i)$	$\theta \downarrow \text{const}$, $\dot{\delta} \downarrow \text{const}$	$\theta \uparrow \text{const}$, $\dot{\delta} \uparrow \text{const}$

This figure "photo.jpg" is available in "jpg" format from:

<http://arxiv.org/ps/cond-mat/0208413v1>